



**KEK Report 96-17**  
**February 1997**  
**A**

# **Design of the JHP 200-MeV Proton Linear Accelerator**

Takao KATO

**NATIONAL LABORATORY FOR  
HIGH ENERGY PHYSICS**

© National Laboratory for High Energy Physics, 1997

KEK Reports are available from:

Technical Information & Library  
National Laboratory for High Energy Physics  
1-1 Oho, Tsukuba-shi  
Ibaraki-ken, 305  
JAPAN

Phone: 0298-64-5136  
Telex: 3652-534 (Domestic)  
(0)3652-534 (International)  
Fax: 0298-64-4604  
Cable: KEK OHO  
E-mail: Library@kekvox.kek.jp  
Internet: <http://www.kek.jp>

# DESIGN OF THE JHP 200-MeV PROTON LINEAR ACCELERATOR

Takao KATO

KEK, National Laboratory for High Energy Physics

Oho 1-1, Tsukuba-shi, Ibaraki-ken, 305, Japan

## Abstract

A 200-MeV proton linear accelerator for the Japanese Hadron Project (JHP) has been designed. It consists of a 3-MeV radio-frequency quadrupole linac (RFQ), a 50-MeV drift tube linac (DTL) and a 200-MeV separated-type drift tube linac (SDTL). A frequency of 324 MHz has been chosen for all of the rf structures. A peak current of 30 mA ( $H^+$  ions) of 400  $\mu$ sec pulse duration will be accelerated at a repetition rate of 25 Hz. A future upgrade plan up to 400 MeV is also presented, in which annular-coupled structures (ACS) of 972 MHz are used in an energy range of above 150 or 200 MeV. One of the design features is its high performance for a beam-loss problem during acceleration. It can be achieved by separating the transition point in the transverse motion from that of the longitudinal motion. The transverse transition at a rather low-energy range decreases the effects of space-charge, while the longitudinal transition at a rather high-energy range decreases the effects of nonlinear problems related to acceleration in the ACS. Coupled envelope equations and equipartitioning theory are used for the focusing design. The adoption of the SDTL structure improves both the effective shunt impedance and difficulties in fabricating drift tubes with focusing magnets. An accurate beam-simulation code on a parallel supercomputer was used for confirming any beam-loss problem during acceleration. Details concerning the design work are described in this paper.

**KEY WORDS:** proton linear accelerator, Japanese Hadron Project, high intensity, beam loss, transition, space-charge effect, computer simulation

Table of contents	Page
1. Introduction	3
2. General concept	3
2.1 Requirements	3
2.2 Design philosophy	5
2.3 Transition	7
3. Accelerating structure	8
3.1 General scheme	8
3.2 Type of accelerating structures	9
3.2.1 RFQ	9
3.2.2 DTL	10
3.2.3 SDTL	11
3.2.4 CCL	12

3.3	Effective shunt impedance	12
3.3.1	ZTT of RFQ	13
3.3.2	ZTT of DTL and SDDL	13
3.3.3	ZTT of CCL	13
3.4	Frequency of the RFQ and low-energy transition energy	15
3.4.1	Boundary condition	15
3.4.2	RFQ and DTL parameters	16
3.5	Accelerating field limit	20
3.6	Details of the accelerating structure	20
3.6.1	ZTT of DTL and SDDL	21
3.6.2	ZTT of the double-frequency SDDL	22
3.6.3	ZTT of CCL	23
3.6.4	Transition energy from the DTL to the SDDL	25
3.6.5	Number of unit cells in an SDDL tank	25
3.6.6	Transition by using CCL	26
3.7	DTL design	34
3.7.1	DTL focusing design	34
3.7.2	Transition energy from the DTL to the SDDL	36
3.7.3	LINSAC simulation for the DTL and the SDDL	39
3.7.4	SDDL simulation with field errors	43
3.8	Beam simulation for studying the transition from the DTL/SDDL to the CCL	43
3.8.1	Transmission	47
3.8.2	Emittance growth	49
3.8.3	Injection beam into the DTL	49
3.8.4	Properties of the code LINSAC	53
3.9	CCL of 648 MHz	58
3.10	CCL of 972 MHz with an injection energy of 100 MeV	59
4.	RF source	63
4.1	Power-dividing method for SDDL unit tanks	63
4.2	Field errors due to a change in the beam current	63
5.	Beam-transport line between the RFQ and the DTL	65
5.1	General design	65
5.2	Buncher	65
5.3	Chopper	65
6.	Debuncher for the output beam	66
7.	Lorentz stripping of $H^-$	66
8.	Upgrade of the output energy	68
9.	Summary of the design	69

# 1. Introduction

A proton linear accelerator for the Japanese Hadron Project (JHP) has been designed. The main features of the requirements for the linac are a high-peak current, a high-average current and a high-duty factor. The expected average current will be 200  $\mu\text{A}$  at the beginning, and nearly 1 mA in the future. These parameters strongly require the best ability of the total system as well as each device of the linac. In addition, since it is to be used as an injector into the following 3-GeV rapid-cycle synchrotron, supplying beams for many kinds of scientific studies, stable operation with the required beam quality during many years is the most important and necessary character of the linac. In order to construct and operate the linac with such a high quality, the design concept is crucially important. Although details concerning the design and construction of each accelerator components are also important, they would not exhibit their best ability if they were to be used according to an incorrect scenario. Both best designs for the total system and the individual excellent accelerator devices can achieve accelerated beams having the best qualities. This paper presents the design of the JHP proton linear accelerator. The final design was determined not only based on the results of a beam-dynamics calculation, but also by careful studies of the accelerating structures, rf devices, and tuning and operation methods. Therefore, the processes of designing as well as the final design are also described here.

## 2. General concept

### 2.1 Requirements for the JHP linac

The required main parameters for the JHP proton linac are listed in Table 1. The construction plan of the linac consists of two stages. In the first stage, a linac of required minimum ability, which can satisfy the injection-beam parameters of the following ring, will be constructed. An upgrade of the linac is being planned from the beginning, and will be gradually performed in

**Table 1** Required main parameters of the linac.

	Initial requirement	Final goal	
Particles	$\text{H}^-$	$\text{H}^-$	
Output energy	200	400	MeV
Peak current	30	60	mA
Beam width	400	400	$\mu\text{sec}$
Repetition rate	25	50	Hz
Average current	200	800	$\mu\text{A}$
Length	<150	~220	m
Momentum spread	$\pm 0.1$	$\pm 0.1$	%

order to increase the average beam current based on the accumulated experience of beam acceleration during operation. Therefore, the future extension plan of the linac should be included in the beginning stage of the design consideration. Negative hydrogens, instead of protons, will be accelerated because of the requirement from the injection scheme into the following ring. This imposes severe restrictions on the beam properties from the ion source, and characterizes the total linac system, since a rather lower peak beam current and a longer pulse length are assumed for an  $H^-$  beam compared with proton acceleration.

### **Output beam of the linac**

An output energy of 200 MeV is required in the first stage of construction. An upgraded energy of 400 MeV is planned for the future. A peak current of 30 mA with a pulse length of 400  $\mu$ sec at a repetition rate of 25 Hz is required in the first stage of construction. There is a future plan to have a peak current of 60 mA, a pulse length of 400  $\mu$ sec and a repetition rate of 50 Hz. In those items, an increase in the repetition rate causes mainly an rf power issue, which means that it requires additional costs for upgrading the rf systems. The increase in the output beam energy requires an extension of the accelerator structure and an additional rf power system. An increase in the peak current involves a beam-dynamics issue as well as accelerating-structure and rf power issues. It is also related to the ion-source capability. The most crucial problem is that there is no  $H^-$  ion source which can produce a peak current of 60 mA with an appropriate transverse emittance and under high-duty operation. In addition, the transverse emittance from the ion source usually increases as the peak current increases. The maximum accelerating current in the RFQ depends upon the operating frequency and the emittance of the injection beam. On the basis of the current technologies of both  $H^-$  ion sources and the RFQ, it seems to be difficult, but not impossible, to accelerate a peak current of 60 mA when an RFQ frequency of 324 MHz is selected. In other words, the design of the injection part of the linac, including a minor modification for a future peak current of 60 mA, becomes realistic if the ion source would supply such a current. On the contrary, a system with two rather low-frequency RFQs, which can accelerate high-intensity beams easily, followed by a double-frequency DTL via a funneling beam line, has been proposed (ref.1). However, when the frequency is again multiplied in the DTL-CCL (coupled cavity linac) transition, the density in the CCL bunch becomes extremely high, resulting in a severe space-charge problem, even in the high-energy acceleration region. Therefore, although the scheme mentioned above seems to be attractive, it requires a further careful investigation for the system with a moderate beam current. In the design of an RFQ and DTL of the same frequency, the high-energy part of the linac can handle an increase in the peak current with an additional rf power increase and with varying the transverse tune. The energy spread of the output beam can be easily controlled to meet the requirements by using a debuncher cavity located a few tens of meters downstream of the exit of the linac. The transverse and longitudinal emittances can be controlled via an equipartitioning process by changing the transverse tune on the basis of the coupled envelope equations for both the transverse and longi-

tudinal motion.

Variable transverse tune is required.

The same frequency for both RFQ and DTL is selected.

### **Length of the linac**

The total length of the linac imposes an important boundary condition on the design of the total system. The available length of 200 m for the maximum output energy of 400 MeV requires an average accelerating energy gain of 2 MeV/m, which seems to be rather high compared with those for conventional accelerators; the LAMPF value is 1 MeV/m. However, the expected additional beam-dynamics problems related to nonlinear effects due to the rather high average accelerating field can be solved by both selecting an appropriate accelerating system and applying equipartitioning acceleration along the linac simulated by using an accurate beam-dynamics computer code.

The total length is limited to about 200 m for a 400-MeV linac.

Finally, the other important requirement, which is not listed in the Table 1, is to achieve stable operation with minimum beam losses in the acceleration of the required current. Although it is difficult to estimate these properties in terms of the figures, our machine should always be designed, constructed, commissioned and tuned from these points of view.

## **2.2 Design philosophy**

Within the framework of satisfying the requirements, our criteria for designing of the linac are as follows:

### **1) Stable operation with minimum beam losses**

The JHP linac should be designed and constructed with appropriate margins for beam losses in order to achieve a stable and reliable operation of the total system, including the accelerating structure, rf power supply, water-cooling system, vacuum system and monitor and control system. An accurate beam-dynamics simulation code, including both an accurate electromagnetic field distribution in the acceleration process and an exact three-dimensional space-charge calculation, should be used for determining the main parameters of the linac, such as the frequencies, type of accelerating structures and transition energies from the viewpoints of not only the rms properties of the beam, but also the behavior of the halo-like particles around the core-part of the beam. An advantage of the code is that it also involves an important simulation of beam behaviors related to beam-halo formation without any artificial approach. Focusing

along the linac is performed based upon the theory of the coupled envelope equations as well as equipartitioning theory. It is a useful method from the viewpoints of obtaining a good beam qualities with the space-charge effects and controlling the emittance-transfer between the transverse and longitudinal phase spaces. Achieving good beam qualities in both the transverse and longitudinal phase spaces is the quickest way to satisfy the requirements of the JHP linac. The type and capability of the rf sources are determined from the viewpoints of reliability during operation.

## **2) Easy tuning for varied peak currents**

One of the important problems in a high-intensity linac is to establish an effective tuning method for various peak beam currents, since the beam-loss problem often becomes serious when the peak current increases. Therefore, it is required to tune the transverse focusing forces freely for all rf structures in order to compensate for any space-charge effects, which in turn determine the highest possible frequencies for the DTL structure. In order to satisfy the requirements, beam diagnostics systems, carefully prepared along the linac, are crucial. Moreover, in order to obtain reliable beam data which can be compared with the calculated results, it is also crucial to construct accelerating structures and to align them within the required accuracy on the basis of the calculation. However, everyone knows its difficulty through long-term experience. It is thus pointed out again that it is important to understand the fact that the accumulation of each part of the linac, accurately designed and fabricated, can make the linac reliable and stable.

## **3) Positive adoption of new ideas and devices**

A long time has passed since the first-generation high-energy proton linacs were constructed. During this long period, many new ideas for proton linacs were proposed and tested. Although many of them were dismissed, some proved to be valid for the future linac technology. Therefore, it is a reasonable way to take these new ideas and devices into our design positively. However, it should be pointed out that a lot of theoretical and experimental studies are required for the adoption and realization of new ideas, since there are some possible differences between the properties obtained in a small test bench and those in a large linac. Thus, if there were a several candidates for a linac component, the merits and demerits of each should be carefully studied and compared.

## **4) Easy maintenance after construction**

The accelerator will supply beams for various scientific research groups for more than ten years. During the long-term operation, many elaborate efforts to maintain and improve the ability of the linac will be required. Thus, the ease of maintenance and modifications should be taken into account during the first design. Although it is difficult to represent these characteris-

tics by figures, the design should be performed on the basis of this criterion.

## 5) Minimum cost

Everyone knows the importance of low-cost construction. However, cost estimations have difficulties in the sense that each designer sets his own boundary on the total-cost estimation. Therefore, it could be possible to construct accelerating structures with minimum cost and with maximum cost for future improvements and modifications. Generally speaking of accelerating structures, although it is possible to improve one of the rf properties greatly, it usually sacrifices other properties, which become serious problem in some cases. Therefore, more careful studies are required whenever a new idea is extremely superior concerning one of the properties. Thus, our cost optimization should be performed based upon the following criteria:

- 1) a simple accelerator structure, both in rf properties and mechanical structure, is desirable, since it leads to reliable and stable operation with the total minimum cost finally,
- 2) including not only the initial and directly required cost, but also the expected future costs for both maintenance and improvements.

## 2.3 Transition

A transition means some abrupt changes in the focusing forces from the previous periodical nature. Therefore, it includes changes in an accelerator structure, an operating frequency and a focusing period. Generally, the beam size changes after a transition according to a change in the focusing forces. Thus, it is desirable from the viewpoint of beam dynamics that the number of transitions be as small as possible. The optimum beam sizes for a certain part of the accelerator are defined by using both the coupled envelope equations and the equipartitioning theory. Here, let us define the optimum beam by the equipartitioning, since the bunch properties vary according to the theory along the long linac. For a high-accelerating field linac, the nonlinear forces of the accelerating field are one of the main reasons for making the beam quality bad. In order to avoid these effects, a relatively shorter bunch length would be desirable. Frequency multiplication usually causes a relatively large bunch length in terms of the rf phase. Therefore, a smaller number of frequency multiplication is desirable. Also, a higher transition energy, where the relative bunch length decreases according to damping theory, is desirable. On the contrary, a lower energy transition is desirable for transverse motion, since a large transverse beam size is desirable from the viewpoint of the space-charge effects. The SDTL focusing method generally provides a larger  $\beta$ -function than that in the DTL focusing method. Moreover, equipartitioning theory predicts an increase in the transverse beam size as the energy increases. Therefore, the transition from DTL to SDTL solves the above-mentioned problem: the transverse focusing changes, while keeping the longitudinal focusing method unchanged. Next, the transition from SDTL to CCL changes the method of longitudinal focusing, keeping transverse focusing un-

changed. In addition, the relative bunch length becomes sufficiently short at the exit of the SDTL, avoiding non-linearity of the accelerating field in the CCL of the multiplied frequency. The bunch length does not vary much along the acceleration. However, the relative bunch length in terms of the rf phase decreases as the energy. The key to solving the transition problem is not to consider the expected beam losses, but to avoid or decrease any beam losses due to the transition. It seems to be contradictory to say that if there were beam losses, low energy would be desirable; thus, a low-energy transition in frequency should be selected in spite of degradation of the beam quality by selecting such a transition. At last, it should be pointed out that an odd number of frequency multiplication factor is desirable if there were needs for a simultaneous acceleration of both protons and negative hydrogens in the future.

### 3. Accelerating structure

#### 3.1 General scheme

The acceleration efficiency can be expressed by the effective shunt impedances (ZTT). The shunt impedance (Z) and the transit time factor (T) are defined as

$$Z = \frac{E_0^2}{P_c / L}$$

and

$$T = \frac{\int_0^L E_z \cos(\omega t) dz}{\int_0^L E_z dz},$$

where  $P_c$  is the dissipation power in an rf structure,  $L$  the length of the structure,  $E_z$  the accelerating field along the center axis of the structure, and  $\omega$  the angular resonant frequency. The average accelerating field is given by

$$E_0 = \frac{1}{L} \int_0^L E_z dz.$$

The effective shunt impedance is defined by

$$ZTT = Z \times T \times T.$$

In a high-energy linac, it is common to adopt a few kinds of accelerating structures with different operating frequencies as the energy increases in order to achieve the highest ZTT totally (we call the changing point a transition). It is pointed out that some crucial problems concerning the beam properties are induced by changing the rf structures and operating frequencies. Since ZTT is expressed in terms of figures, it seems to be more persuasive than a qualita-

tive discussion about additional beam problems due to the installation of transitions. Therefore, it seems to be quite reasonable that the optimization of the total ZTT is stressed for a low-average beam intensity linac, in which some of the possible beam losses along the linac cause no serious radioactive problem. In such a linac the driving power is much larger than the beam power. However, for a high-intensity linac, minimization of the beam losses is much more important than optimization of the total ZTT. Unfortunately, the two optimization mentioned above are not compatible with each other according to my knowledge. Recently, progress in accurate beam-simulation codes can reveal the effects of a transition upon the beam properties. Therefore, our criteria for selecting the main linac parameters depend upon both beam-loss minimization by a beam-dynamics simulation and ZTT optimization. In general, a higher frequency is desirable from the viewpoint of ZTT and the effects of space-charge. There are many items which characterize the accelerating structures. They are discussed in detail for each accelerating structure in the following sections.

### **3.2 Type of accelerating structures**

The possible candidates for the accelerating structures are as follows:

- 1) RFQ (radio frequency quadrupole),
- 2) DTL (drift tube linac),
- 3) SDTL (separated-type drift tube linac) and
- 4) CCL (coupled cavity linac).

It should be noted that the frequency dependence of both the transverse acceptances and the effective shunt impedances depend upon the types of structure. For example, the transverse acceptance for DTL does not depend upon the operating frequency if the mechanical sizes are properly chosen according to the scaling law. On the contrary, it does not depend upon the frequency only when the bore radius and the length for the focusing period hold constant in spite of different frequencies in the case of CCL. Thus, the frequency dependence of the ZTT in such structures is different from that for scaled structures, such as DTL. For high-intensity linac's use, a sufficiently large transverse acceptance is necessary, resulting in a deviation of frequency dependence of ZTT from the normal scaling law due to the rf resistivity. This nature arises from the fact that the rf invasion into the bore part depends upon the ratio of the bore radius to the wavelength.

#### **3.2.1 RFQ**

The RFQ of the four-vane type is a candidate for a low-energy injection part of the linac. It has many good properties due to both focusing and acceleration with an rf electric field. However, this property becomes disadvantage when free tunings of both the transverse and

longitudinal beam motion are required, since it is impossible to tune one motion without changing the other motion. It is widely seen that there is some uncertainty concerning the field distribution related to a two-dimensional cutting method of the vane geometry. Here, we also encounter the situation that another beam-acceleration problem is generated by decreasing the fabrication cost and increasing the rf properties related to a discharge problem. In short, there is a large discrepancy between the accelerating fields produced by the real vane geometry and a theoretical prediction using a three-dimensional calculation. The amount of correction of the field deviation is more than a few decades of percent, and it is difficult to directly measure the field distribution. A further investigation concerning the accelerating field is desirable in order to clarify the acceleration process in the RFQ. This is because accurate knowledge about every device is indispensable for achieving stable operation of the total linac system with reliable tuning. As for the transverse-mode stability in an RFQ structure, the PISL ( $\pi$ -mode stabilizing loop) shows excellent rf properties (ref. 2). For high-duty-factor operation, its superior capability for water-cooling is more advantageous.

### 3.2.2 DTL

The DTL is widely accepted for acceleration from low-to-medium energies in a high-energy proton linac. From the viewpoint of a higher shunt impedance, a high-frequency structure is desirable. However, it is impossible to incorporate electroquadrupole magnets into the drift tubes in a rather high-frequency DTL, since the required magnetic-field strength is proportional to the square of the frequency, and the optimum radius of the drift tube decreases in inverse proportion to the frequency. In this case, although some methods can decrease the required magnetic-field strength, they also sacrifice some other properties. For example, the adoption of a small bore radius or focusing elements for every other drift tubes greatly reduces the acceptance. If the permanent quadrupole magnets are adopted for the focusing elements, it is impossible to vary the transverse tune. Since the required magnetic field is inversely proportional to the velocity of the beam, an extension of the RFQ output energy by more than 5 MeV has been considered. However, an energy of 3 MeV is recommended for the JHP linac for the following three reasons:

- 1) a new problem of accelerating tuning with insufficient knowledge of accelerating fields arises by introducing two or three RFQ tanks connected in series in order to increase the output energy. This results in almost blind operation, or operation with only experience, which is in conflict with our second philosophy (mentioned in section 2.2),
- 2) a radiation problem due to using a fast beam chopper should be avoided and
- 3) the efficiency of the RFQ acceleration decreases rapidly as the energy increases.

In addition, the 3-MeV RFQ in JHP test stand recently proved its high performance (ref. 3).

The emittance-growth problem due to space charge in a linac has been studied for a long time, resulting in a new focusing approach in the DTL. This focusing approach depends upon the control of the equipartitioning process among three freedoms of the kinematic motion of

particles in a bunch. Another aspect of the effect of space charge related to beam-halo formation is also an important issue from the viewpoint of beam losses. Here, a new simulation code can be used to find the optimum parameters of the acceleration process, in which beam-halo production can be minimized. Transient beam loading is also important from the viewpoint of the beam properties in a high-peak current linac. Since the DTL operates at zero mode, where the theoretically defined group velocity of the rf operating mode is zero, some devices (post couplers) for stabilizing the long tank are required (ref. 4).

### 3.2.3 SDTL

An SDTL (ref. 5) has a similar structure to a DTL, except for the focusing magnets in the drift tubes (Fig. 1). The focusing magnets in the drift tubes impose severe restrictions on the optimization of the shape of the DTL from the viewpoints of both the ZTT and the transverse acceptances, and on the fabrication of the drift tubes. Therefore, it is natural and reasonable to exclude magnets from the inside of the drift tubes and to place them between two adjacent tanks, which is a similar method to that used in the CCL structure. Then, the optimization of the SDTL geometry can be performed much more freely, resulting in a higher ZTT compared with that for the DTL. In this case, the additional drift spaces between the SDTL tanks cause new beam-dynamics problems, mainly in the longitudinal motion. This effect becomes larger as the energy decreases. The period of the transverse focusing changes at the transition point from DTL to SDTL, resulting in the requirement of a transverse matching section between them. However, this transition can be interpreted as one which moves down from the transverse transition from the DTL to the CCL in the conventional constitution of a high-energy linac. In fact, introducing the SDTL structure causes a separation of the transverse transition point from that of the longitudinal one. The effects of the separation of both transition points should be investigated using a beam-dynamics simulation described in the following sections. Because of the simple structure

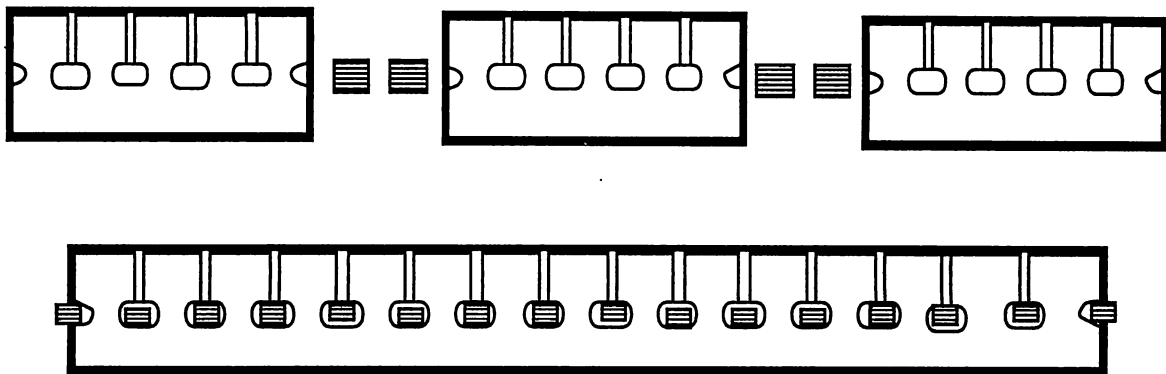


Fig.1 SDTL (upper) and DTL (lower) structures. The focusing magnets are indicated by squares.

of the SDTL tank, the fabrication and alignment of the drift tubes and tanks become easier compared with that of a conventional DTL, resulting in a reduction in the construction cost as well as a reduction in the number of focusing magnets. Moreover, since a unit tank of the SDTL consists of several unit cells, stabilizing devices are not necessary, resulting in a more simple structure compared with the DTL, as well as a reduction in the construction cost. The maintenance work after construction will be also greatly reduced because of the simple structure.

### 3.2.4 CCL

Many types of structures for the CCL have been proposed and studied; some of them have been used in the high-energy part of the linac (LANL, INR, FNAL). According to the long term development for CCL structures at KEK, it is concluded that the ACS (annular-coupled structure) is suitable for a high-energy accelerating structure from the viewpoints of the axial symmetric property of the electromagnetic field in the structure and stable operation without any discharge problem (ref. 6). The effective shunt impedance of the CCL decreases as the energy decreases because of the existence of walls between two adjacent cells and coupling cells on the beam axis in some types of structures. The effect is more serious for a high-duty factor CCL, since the required wall thickness between two adjacent cells for water cooling becomes relatively very large in a low- $\beta$  structure. As for an on-axis coupled structure (OCS), its ZTT is always smaller than that of the SCS (side-coupled structure) and the ACS, because of the existence of space due to coupling cells. It should be stressed that many properties other than ZTT are also very important for a high-duty factor structure, since a high ZTT can usually be achieved at the cost of performance under high-duty factor operation.

### 3.3 Effective shunt impedance

The effective shunt impedance is one of the important factors if the rf power loss in a structure is not very small compared with the beam power. It is normally proportional to the square root of the operating frequency because of the property of high-frequency rf resistivity. Thus, a higher frequency is generally more advantageous.

In order to compare the effective shunt impedances for different types of accelerating structures of different operating frequencies, a careful consideration of many items is required, because the effective shunt impedance achieved in a realistic structure depends upon many factors which are determined by both the properties of the rf fields and the mechanical conditions for fabrication. Therefore, it is widely accepted that the shunt impedances are first calculated for the idealized and realistic shapes, and any decrease in the effective shunt impedances due to many effects are secondly considered as perturbations. The reasons for the additional decrease for each type of structure are considered in the following sections.

### **3.3.1 ZTT of RFQ**

Since an RFQ is not very long in length and has special functions of bunching, focusing and acceleration by an rf field, which can not be found in other types of structures, the effective shunt impedance, as well as an additional rf power-loss problem associated with VCR or PISL, is considered to be rather trivial compared with the other superior functions mentioned above, especially for a high-intensity RFQ.

### **3.3.2 ZTT of DTL and SDDL**

#### **1) Effect of stems**

The support stems of drift tubes cause additional rf power losses, which are proportional to the radius of the stem. It reaches approximately a few percent of the power loss for the conventional DTL geometry.

#### **2) Effect of both end plates of the unit tank**

Since the number of unit cells for an SDDL tank is not very large, the additional rf power losses due to both end plates are not negligibly small compared with the total power loss in the tank. The ratio of the additional loss depends upon the number of cells within a tank. It is approximately 20% for a five-cell SDDL structure.

#### **3) Effects of post-couplers**

The post-couplers used for stabilizing the DTL structure cause additional power losses, that are approximately equal to those due to the stems.

#### **4) Effect of phase slip**

There is no additional decrease in the acceleration efficiency in the DTL due to a phase slip within a tank, since a varied-beta structure (the unit-cell length corresponds to the stable-particle energy in the cell) is used. The varied-beta cell structure is also suitable for an SDDL structure, because the merits for adopting a constant-beta cell structure (all cell length in a tank are equal) are not very large. Since the number of unit cells in an SDDL tank is not large (several cells at maximum), a reduction in the fabrication cost associated with the constant-beta cell structure can not be expected.

### **3.3.3 ZTT of CCL**

#### **1) Effect of the coupling coefficients**

A coupling between two adjacent cells in the coupled cavity structure causes an additional power losses compared with the calculated results with only an accelerating cell geometry. It

depends upon the coupling values: a 20% reduction for a 5% coupling coefficient for the 1296-MHz ACS structure (ref. 6). Thus, a stable operation for a high-peak current can be achieved with both high coupling coefficients and an associated additional decrease in the effective shunt impedances.

## 2) Effect of phase slip

Since the number of unit cells in a CCL tank is not very small, because of the adoption of the  $\pi/2$ -mode operation and the selection of a higher operating frequency, it is widely accepted that it is more advantageous (mainly from the viewpoint of construction cost) to make a CCL structure with a constant- $\beta$  structure, which means that the unit-cell length holds constant through the unit tank. Therefore, some phase slips are expected during acceleration, causing an additional decrease in the efficiency of the acceleration. There is a method to recover the acceleration efficiency by choosing a smaller injection stable phase angle (in terms of absolute value) in a tank; however, it can be performed by producing an additional beam-dynamics problem: a decrease in the longitudinal acceptance and more complicated phase oscillations. The ratio of the decrease in the acceleration efficiency depends upon both the particle energy and the average accelerating field, reaching an order of 10%. The effects become smaller when the particle energy increases and the energy gain per unit length becomes smaller. The selection of a small number of unit cells in a tank for decreasing the effects causes an increase in both the number of unit tanks and the drift space, resulting in bad effects on the longitudinal motion.

## 3) Effect of the wall thickness between two adjacent unit cells

Water cooling for the inner surface of the unit cells in a CCL tank is indispensable for a high-duty factor structure. It should be stressed that the required minimum thickness of the wall between two adjacent cells be nearly constant for CCL structures of different energies and different frequencies. Therefore, the effects of the wall thickness on the effective shunt impedance become larger as the energy decreases and the frequency increases. In addition, the amount of the effects depends upon the type of structure, since there are some kinds of structures in which mechanical deformation due to a rise in the temperature around the nose-corn region causes a severe deformation of the coupling cell geometry, resulting in a deviation of the coupling cell frequency and a decrease in the performance. Therefore, it is pointed out that the deformation due to the distribution of the temperature in an accelerating structure should be carefully investigated for a high-duty factor structure. Critical operation without a cooling channel and a smaller safety margin should be avoided.

## 4) Effect of the bore radius

It is commonly accepted that the transverse focusing elements for the CCL-type structures should be placed between two adjacent tanks. In such a configuration, the transverse acceptance is determined by three factors: the phase advance, bore radius, and length of the focusing period. Thus, it is stressed that it usually does not depend upon the rf frequencies. It is also commonly

accepted that a small number of total tanks is more desirable from the viewpoints of both the rf equipment and the total costs. However, a tank of long length means a long focusing period, resulting in a decrease in the transverse acceptance, which can be compensated by enlarging the bore radius. A relatively large bore radius, compared with the wavelength, causes more invasion of the rf field into the bore part of the structure, resulting in a decrease in the transit time factor. The ratio of the decrease depends upon both the ratio of the bore radius to the wavelength and the corresponding energy range. Generally, a higher frequency and a lower energy have large effects.

### 5) Effect of a stable phase angle

When the operating frequency is multiplied at a lower energy region, it is inevitably necessary to adopt a larger stable phase-angle (absolute value) in order to accept all particles. The acceleration efficiency, including the stable phase angle, is defined as

$$ZT^2 \cos^2 \phi_s = \frac{(\Delta W)^2}{P_c L},$$

where  $\Delta W$  is the energy gain and  $\phi_s$  is the stable phase angle. Therefore, the efficiency of the acceleration decreases effectively, for example, by 27 and 49% for acceleration with a -40 or -50 degree stable-phase-angle, compared with that with -26 degrees. The amount of degradation is not negligibly small.

In conclusion, the total amounts of the decreases in ZTT for the idealized geometry are roughly equal for the SDTL and CCL structures. For a five-cell SDTL at an energy of 100 MeV, it becomes about -18%; -13% due to both end plates and -5% due to the stem. For the ACS, the average decrease is about -30% ; -20% due to 5% coupling and -10% due to phase slip. The decreases due to both the phase slip and a lower stable phase angle are automatically taken into account in the calculated results. Therefore, we compare the ZTT which does not include any corrections mentioned above, since the final conclusion does not depend upon such details. It is noted that a factor of 1.2 - 1.3 is taken into account in the rf driving-power calculation in this paper.

## 3.4 Frequency of the RFQ and low-energy transition energy

### 3.4.1 Boundary condition

The boundary conditions for selecting the operating frequency and the transition energy in the injection part of the linac are summarized as follows:

- 1) A higher frequency is desirable from the viewpoint of the space-charge effect.
- 2) A single-tank RFQ is desirable.

- 3) A higher output energy of the RFQ is desirable, since the required focusing magnetic field gradient for the DTL decreases in inverse proportion to the velocity of a particle.
- 4) The same frequency for the RFQ and the following structure is desirable, since it is important to decrease the number of particles in a bunch from the viewpoint of space-charge effects.
- 5) A lower frequency is desirable from the viewpoints of the transverse acceptances and the maximum current limit for the RFQ.
- 6) Tunable transverse focusing elements for the structure placed after the RFQ are required.
- 7) A matching section is used between the RFQ and the following structure. It is also used for installing a fast beam chopper, which is helpful for decreasing beam losses in the following ring.
- 8) A lost beam by the fast beam chopper does not cause strong radioactivity.

The threshold values for the neutron yield by protons are 4.15 MeV for  $^{63}\text{Cu}$  (69% probability), 2.13 MeV for  $^{65}\text{Cu}$  (31% probability) and 5.61 MeV for  $^{27}\text{Al}$ . The yield ratios from Cu by 3 and 5.4 MeV-protons are  $1.61 \times 10^6$  and  $2.81 \times 10^8$  n/sec/mA, respectively (ref. 7).

- 9) The system configuration with a CCL-type structure placed just after the RFQ shows no merit from the viewpoints of beam dynamics and accelerating efficiency.
- 10) An SDTL-type structure placed immediately after the RFQ shows no merit from the viewpoint of both the transverse and longitudinal beam dynamics.
- 11) A klystron can be used as an rf power source.
- 12) From the viewpoint of beam-halo formation due to the space-charge effects, a rather low frequency is desirable. However, there is still no evidence of a strong frequency-dependence for halo-formation from the results of an accurate beam simulation.
- 13) A small number of the operating-frequency multiplication factor at the transition is desirable from the viewpoint of avoiding a nonlinear rf force in the following rf structure.
- 14) A sufficiently large transverse acceptance compared with the beam emittance is desirable.

### 3.4.2 RFQ and DTL parameters

A reasonable and simple solution for the injection part of the linac, based upon the conditions mentioned in section 3.4.1, comprises a complex of a single RFQ tank followed by a DTL tank via a matching beam-transport line; both operate at the same frequency. In order to obtain a sufficiently large acceptance of the DTL, an FD focusing system with variable electroquadrupole magnets is desirable. Within the framework of a normal conducting magnet, there is a limit on the maximum magnetic field on the surface of the pole-tip, which, in turn, determines the possible highest frequency for the DTL. The RFQ tank length is closely related to the output energy

of the RFQ. The highest output energy by using a single RFQ tank (about 3 m long) is desirable. As a result of the consideration mentioned above, a frequency of 324 MHz is recommended. It corresponds to one fourth of 1296 MHz, which is familiar to us due to long-term studies concerning CCL structures and a high-power rf power source. An RFQ with an output energy of 3 MeV is recommended. A lost beam in the beam-transport line between the RFQ and the DTL by a fast beam chopper gives a small yield of neutrons in this energy range. Details of the discussion are given below.

### 1) Length of the RFQ versus the output energy

The RFQ length as a function of the output energy by a preliminary calculation is given in Fig.2. The calculation was performed based on the assumption of an injection energy of 50 keV and a maximum vane-voltage of 1.8-times the Kilpatrick field limit (17.8 MV/m for 324 MHz).

### 2) Required focusing field gradient at the DTL injection

The required focusing field gradient ( $B'$ ) for a zero-current transverse-phase advance ( $\sigma_0^t$ ) is given by

$$B' = \frac{mc\beta\gamma\theta_0^2}{qL^2} = \frac{W_0\gamma\theta_0^2}{c\beta\lambda^2},$$

$$\theta_0^2 = \left[ \frac{1 - \cos \sigma_0^t - 2\Delta}{\Lambda^2(1/2 - \Lambda/3)} \right]^{1/2},$$

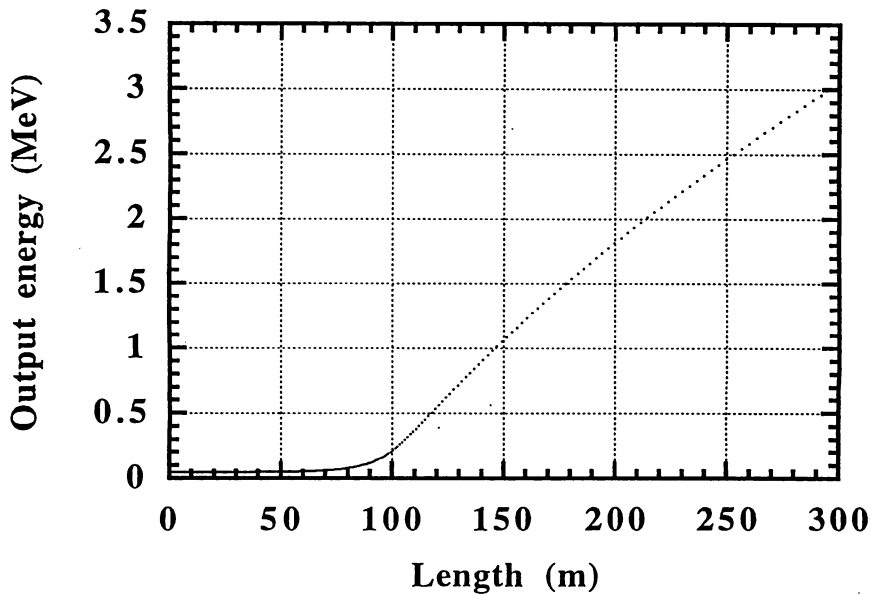


Fig. 2 RFQ length as a function of the output energy at a frequency of 324 MHz.

$$\Lambda = \frac{\ell}{L},$$

where  $m$  is the proton mass,  $c$  the light velocity,  $\beta\gamma$  the usual kinematic parameters,  $\lambda$  the wavelength,  $\Delta$  the effect of the rf defocusing force and  $\Lambda$  the ratio of the length of the quadrupole magnet ( $\ell$ ) to the unit-cell length ( $L$ ). The required field gradient for a zero-current phase advance of 60 degrees as a function of the frequency is shown in Fig. 3. The maximum magnetic field on the surface of the pole is also important in the sense that it relates directly to difficulties in constructing the quadrupole magnets. Therefore, the bore radius is also important from the viewpoints of the construction of quadrupole magnets and the achieved maximum transverse acceptance. The transverse acceptance ( $A$ ) for the FD lattice in the DTL is given by

$$A = \frac{\pi a_0^2}{\beta_{\max}},$$

where  $a_0$  is the bore radius and  $\beta_{\max}$  is the maximum of the  $\beta$ -function, which is proportional to the wavelength. Therefore, the transverse acceptance is independent of the frequency, provided that the bore radius is chosen to be proportional to square root of the frequency. This is a reasonable determination of the bore radius, since the ratio of the beam size to the bore radius is constant for all of the frequencies, and a higher ZTT is obtained by choosing a smaller bore radius (compared with that determined in proportion to the wavelength). These parameters are summarized in Table 2 for five kinds of operating frequencies at an injection energy of 3 MeV.

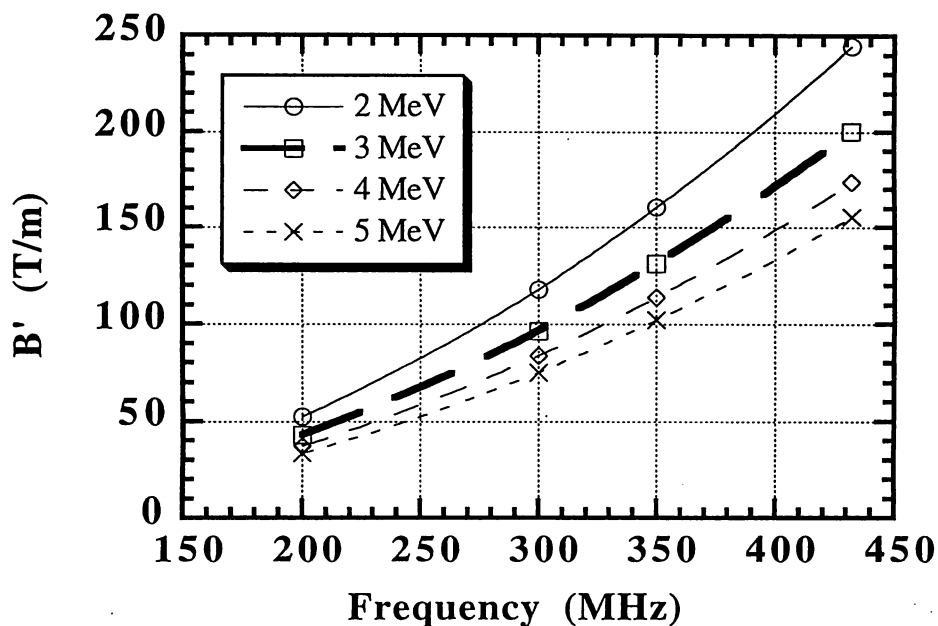


Fig.3 Required magnetic field gradient at the entrance of the DTL for a transverse phase advance of 60 degrees.

**Table 2 Parameters related to transverse focusing vs. frequencies in a 3-MeV injection into the DTL.**

Frequency MHz	Cell length mm	$\beta_{\max}$ m	Bore radius mm	Q-mag radius mm	B' T/m	Bsurface kG
201	119.0	0.395	9.37	11.37	43.4	4.94
300	79.7	0.264	7.67	9.67	96.7	9.35
324	73.8	0.245	7.38	9.38	112.7	10.6
350	68.3	0.227	7.10	9.10	131.6	12.0
432	55.4	0.184	6.39	8.39	200.4	16.8

**Table 3 Typical parameters of the DTL and SDTL structures at a frequency of 324 MHz and an energy of 50 MeV ( $\beta=0.31$ ).**

	DTL	SDTL	
Tank diameter	56	52	cm
DT diameter	13	9	cm
Bore radius	1.3	1.5	cm
Outer corner radius	2.5	2.2	cm
Inner corner radius	1.0	0.5	cm
Z	78.2	75.9	M $\Omega$ /m
T	0.703	0.830	
ZTT	38.6	52.3	M $\Omega$ /m
Esurface peak	4.02	5.87	MV/m

A difficulty in constructing the quadrupole magnet increases if the density of the magnetic flux exceeds 1.8 to 2.2 Tesla (depends upon materials). Thus, a 3-MeV injection scheme from RFQ to DTL at an operating frequency of 324 MHz is selected. If a higher frequency is selected, the construction of the electroquadrupole magnet at 3 MeV becomes impossible, resulting in the selection of a higher injection energy into the DTL. The injection method with a higher RFQ output energy and a higher rf frequency is abandoned because of the boundary conditions of No.2, 5 and 8 given in section 3.4.1. In addition, the diameter of the drift tube becomes relatively larger compared with the wavelength in order to contain a quadrupole magnet, resulting in a decrease in ZTT and a loss of reasonable proportionality between the diameters of the tank and the drift tube. The main parameters are summarized in Table 3.

The maximum emittance of about 3.0  $\pi$ mm-mrad (100%) for a 30-mA RFQ output beam is assumed. Since the transverse acceptance of the DTL is about 42  $\pi$ mm-mrad, a sufficient tolerance for the ratio between the transverse beam size and the bore radius can be realized. The

focusing method along the linac is described in section 3.7.1.

A 3-MeV RFQ followed by a DTL is chosen.  
An operating frequency of 324 MHz is selected for both structures.

### 3.5 Accelerating field limit

The following is a useful measure for the limit of the electric field (Kilpatrick field limit):

$$f = 1.64 \times 10^4 V^2 \exp\left(-\frac{0.085}{V}\right),$$

where  $f$  is the frequency in MHz and  $V$  is the voltage in MV/cm. The calculated values are shown in Fig. 4 and summarized in Table 4. We set the limit for the surface field of the DTL and CCL structures below 1.3-times the Kilpatrick limit according to the experience rule.

### 3.6 Details of the accelerating structure

There are several options for selecting the accelerating structures for a medium energy up to 200 MeV, as follows:

- 1) All DTL structure of the same frequency (ALL DTL),
- 2) A DTL followed by an SDTL (DTL+SDTL),
- 3) A DTL followed by an SDTL and a CCL (DTL+SDTL+CCL) and
- 4) A DTL followed by a CCL (DTL+CCL).

An optimized set of structures should be determined by criteria given as follows:

**Table 4 Kilpatrick field limits for the main frequencies.**

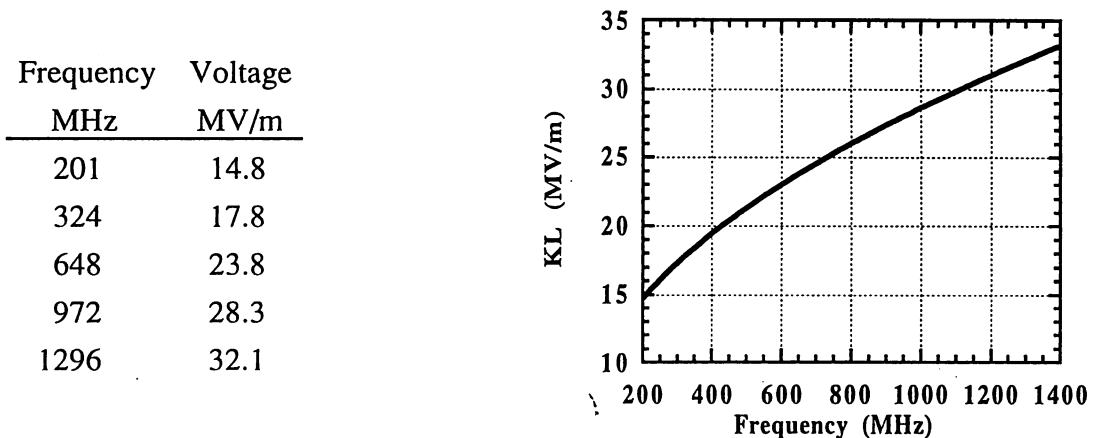


Fig.4 Kilpatrick field limit as a function of the frequency.

- a) satisfactory calculated results by beam-dynamics simulations,
- b) cost optimization from the viewpoint of constructing the accelerator structures and rf power sources,
- c) the possibility of stable and reliable operation for a high-intensity, high-duty factor operation and
- d) a smooth and flexible extension for future upgrades up to 400 MeV.

A DTL structure has been used for acceleration up to 200 MeV in conventional linacs. However, its effective shunt impedance decreases rapidly as the energy increases. Thus, a CCL in an energy region above 100 MeV was introduced in some facilities. At the same time, the operating frequency was multiplied by a factor of some integer in order to utilize the high-shunt-impedance property more efficiently. In the case of acceleration up to 200 MeV, the introduction of a higher frequency seems to be unreasonable because of three reasons:

- 1) the advantage of a higher shunt impedance is lost in the low- $\beta$  region,
- 2) the demerits of introducing the transition seem to be larger compared with the merits of the transition, because the length for acceleration with a higher frequency is short and
- 3) the rf system becomes complicated by using two rf systems with different frequencies, resulting in a bad performance in cost and maintenance work.

The desirable number of the frequency multiplication factor is below three, since the longitudinal motion seems to be dangerous when using more than a factor of four (see section 3.8.1) for a high-intensity linac. A detailed discussion is given below.

A frequency of 324 MHz is used up to 200 MeV.

### 3.6.1 ZTT of DTL and SDTL

Figure 5 shows the ZTT of DTL and SDTL at a frequency of 324 MHz. A SUPERFISH calculation was performed using an ideal geometry without the effects of stems, post couplers and end plates. It is noted that a large radius of the drift tube (70 mm) in the low-energy range is assumed in the calculation because of the installation of an electroquadrupole magnet. On the contrary, the ZTT for the SDTL is freely optimized, resulting in a higher ZTT than that of the DTL. A bore radius of 15 mm is assumed in order to obtain a sufficient transverse acceptance for the SDTL structure. The power-loss ratio due to both end plates to the total power loss becomes large for the SDTL structure, since the number of unit cell is not very large (Fig. 6). The ratio of the reduction of the ZTT due to the rf power loss of the end plates amounts to -13% for the five-cell 100-MeV SDTL structure. The typical geometries are summarized in Table 3. In conclusion, the SDTL is advantageous over DTL in almost all energy ranges from the view-

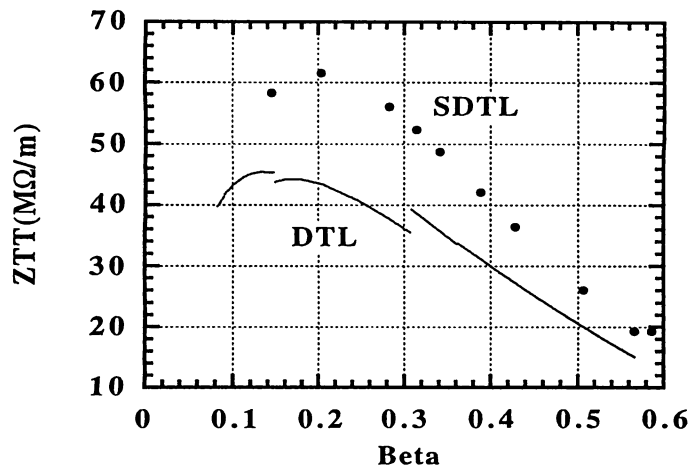


Fig.5 ZTT of 324-MHz DTL and SDTL structures. 'Beta' represents the normalized velocity ( $v/c$ ).

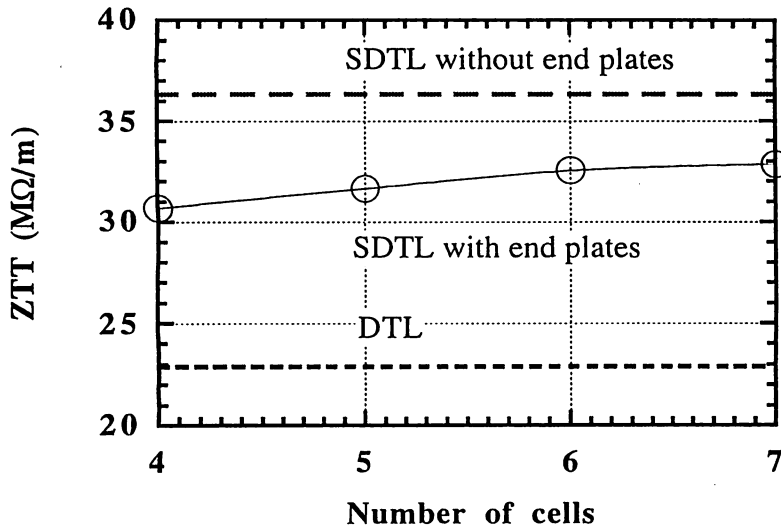


Fig.6 A decrease in the ZTT of the SDTL due to both end plates as a function of the number of unit cells in a unit tank.

point of ZTT-optimization.

### 3.6.2 ZTT of the double-frequency SDTL

The effective shunt impedance of the double-frequency SDTL (648 MHz) is shown in Fig. 7. It is rather surprising that ZTT (648 MHz, bore radius of 15 mm) is nearly comparable with those of the 324-MHz SDTL. This is due to the large bore radius in order to obtain a sufficiently large transverse acceptance, resulting in a decrease in the transit time factor because of an invasion of the rf field into the bore part. On the contrary, the ZTT of the 648-MHz SDTL with a

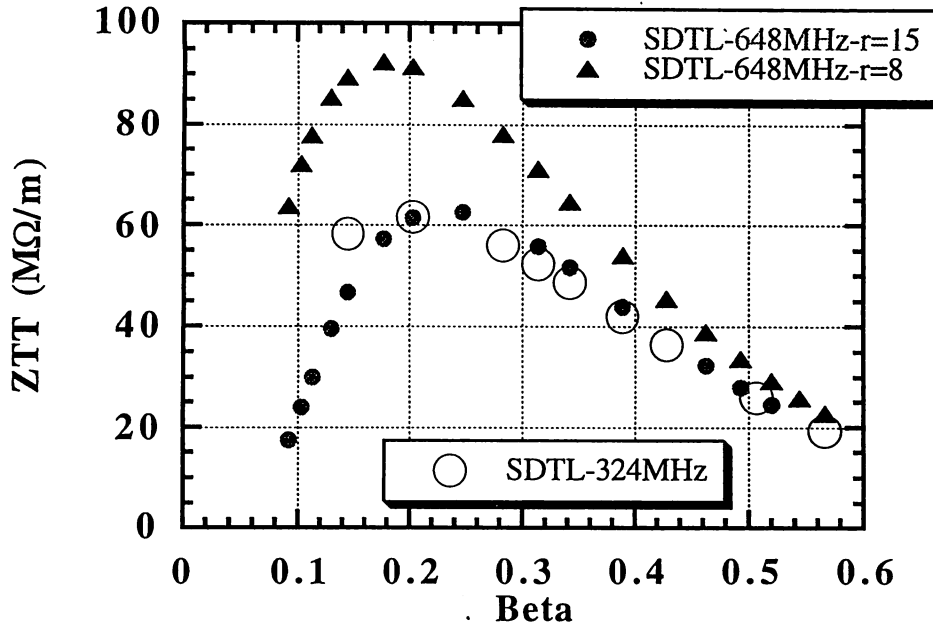


Fig. 7 ZTT of 324 MHz and 648 MHz SDTL structures. Bore radii of 8 and 15 mm for the 648-MHz structures are assumed.

bore-radius of 8 mm is sufficiently high. Therefore, it can be concluded that there is no merit of a higher ZTT in adopting the double-frequency SDTL structure, provided that a structure with a sufficiently large transverse acceptance is required.

### 3.6.3 ZTT of CCL

Three types of coupling cell linac structures are considered: an annular-coupled structure (ACS), a side-coupled structure (SCS) and an on-axis coupled structure (OCS). The optimized accelerating cell geometries for these three are nearly the same. In the case of OCS, the existence of a coupling cell on the beam axis causes a decrease in ZTT. The effects becomes larger for both a lower- $\beta$  structure and for a structure with a water-cooling channel inside of the web. Thus, we first calculate ZTT for the ACS structure. We then take into the effects of the coupling cell of OCS without a water-cooling channel. Thirdly, the ZTT of the OCS with a water-cooling channel is considered. From the viewpoints of stable and reliable operation for a long period of time and the requirement for fabrication, a realistic geometry, which has a sufficiently large wall thickness for cooling and fabrication, should be considered. Two frequencies of 648 and 972 MHz, two and three times the DTL frequency, are assumed. From the viewpoint of a simultaneous acceleration of two kinds of particles, negative hydrogen and protons, an odd integer for the frequency multiplication factor is preferred, since it requires no additional devices for the

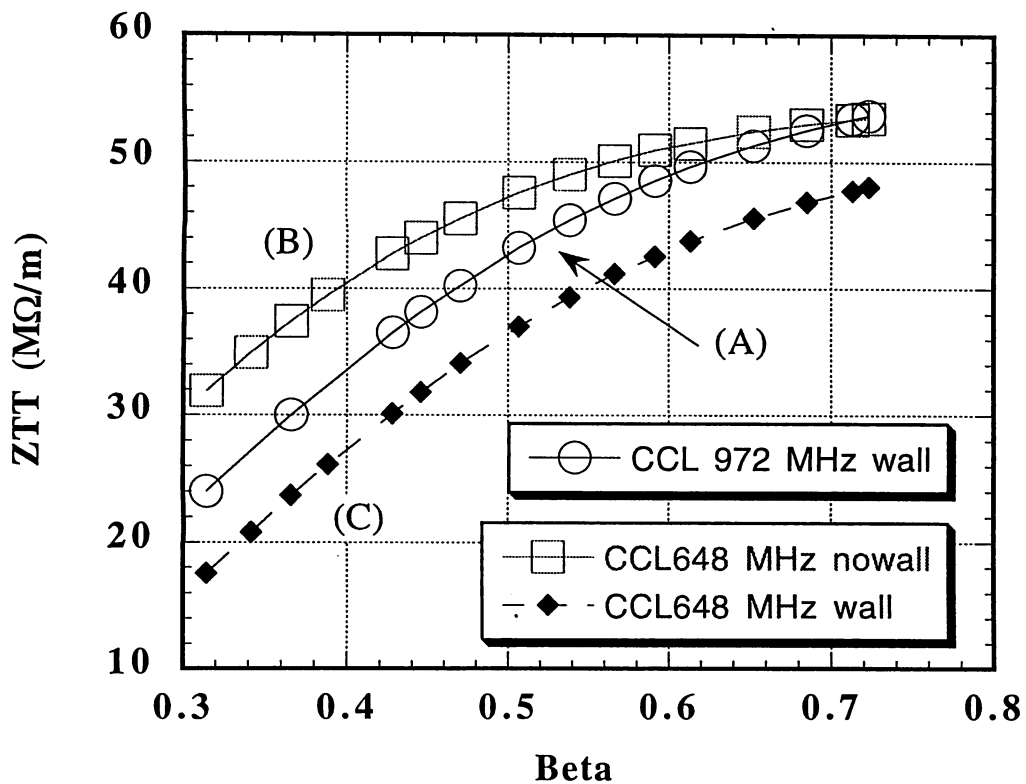


Fig. 8 Calculated ZTT for CCL structures. Line (A) corresponds to the ACS structure with a cooling channel. Line (B) corresponds to an OCS structure without a cooling channel. Line (C) correspond to an OCS with a cooling channel. A bore radius of the CCL is 15 mm.

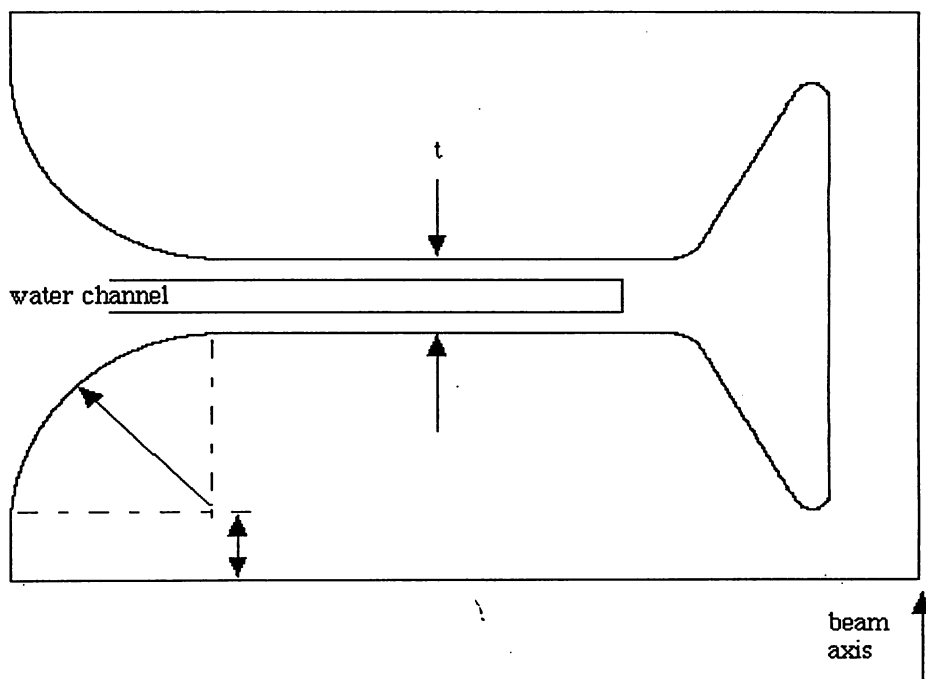


Fig. 9 Typical cell geometry of the CCL-type structure.

DTL-CCL transition region. For the even-integer case, an adjustment of the drift length is required in order to match all of the micro-bunches into the CCL longitudinal acceptance.

The calculated ZTT for an ACS of 972 MHz and an OCS of 648 MHz are shown in Fig. 8. The typical cell geometry is shown in Fig. 9. It is clear from curves (B) and (C) in Fig. 8 that the cooling channels inside of the web parts between two adjacent accelerating cells cause a larger decrease in ZTT as the energy decreases.

### 3.6.4 Transition energy from the DTL to the SDTL

A transition in both accelerating structures and operating frequencies usually causes two kinds of transitions in transverse and longitudinal motions at the same time. On the contrary, a transition from the DTL to the SDTL at the same frequency as that of the DTL causes only a transverse transition. Thus, there is no additional longitudinal problem, except for the effects of a short drift space between the DTL and the SDTL for matching the transverse motion. It is noted that the longitudinal motion is described in terms of the length normalized by  $\beta\lambda$ , and that the required minimum drift space for beam-matching or beam-diagnostics devices is nearly independent of the particle energy. Thus, the effects of the drift space become larger as the energy decreases. In addition, the space-charge effects become smaller as the energy increases. Therefore, a lower transition energy is desirable from the viewpoint of ZTT-optimization, and a higher one is desirable from the viewpoint of longitudinal beam dynamics. Finally, the transition energy is adjusted so that the energy spread of the output beam may be smallest, which strongly depends upon the shape of the longitudinal emittance at the exit of the DTL.

### 3.6.5 Number of unit cells in an SDTL tank

The number of unit cells in an SDTL tank is related to other main parameters as follows:

- 1) the transverse acceptance,
- 2) the longitudinal emittance of the beam,
- 3) the required rf driving power for a tank,
- 4) a decrease in ZTT due to the effects of both end plates of the tank and
- 5) the number of SDTL tanks, focusing magnets and rf components in the total system.

Needless to say, it is concluded that all of the items, except for first one, require a larger number of unit cells in an SDTL tank. Thus, a larger number of unit cells is chosen so long as the transverse acceptance is sufficiently large. Here, we assume that the number of unit cells in an SDTL tank remains constant throughout the SDTL system, since an abrupt change in the length of a focusing period is not good for the beam motion. We also assume a doublet focusing system in order to not only achieve a sufficiently large transverse acceptance, but also to achieve an appropriate shape of the transverse acceptance.

### 3.6.6 Transition by using CCL structure

The main parameters of the transition from DTL/SDTL to CCL are as follows:

- 1) frequency of the CCL,
- 2) transition energy from the DTL to the CCL and
- 3) type of CCL structure.

As stated before, if the output energy is limited to 200 MeV, introducing a CCL structure with a higher operating frequency is not desirable (see section 3.6). However, within the framework of future upgrades up to 400 MeV, the total system would be more efficient by introducing a transition from the DTL/SDTL to the CCL. In such a case, we have the following two candidates for the configuration:

- a) DTL followed by SDTL and CCL,
- b) DTL followed by CCL.

Three types of CCL are being considered: ACS (972 MHz), OCS-I (648 MHz, with water cooling in the nose-corn part), OCS-II (648MHz, without water cooling in the nose-corn part). Since each configuration has freedom of a frequency multiplication factor and the transition energy, there are a number of configurations, assuming two frequency multiplication factors (two and three) , two output energies (200 and 400 MeV) and four transition energies (70, 100, 150 and 200 MeV).

The possible configurations of the linac complex for an output energy of 200 MeV are as follows:

- 1) DTL(324MHz, 55MeV) + SDTL(324MHz, 200 MeV),
- 2) DTL(324MHz, 55MeV) + SDTL(324MHz, 150 MeV) + ACS(972MHz, 200MeV),
- 3) DTL(324MHz, 55MeV) + SDTL(324MHz, 100 MeV) + ACS(972MHz, 200MeV),
- 4) DTL(324MHz, 55MeV) + SDTL(324MHz, 100 MeV) + OCS(648MHz, 200MeV),
- 5) DTL(324MHz, 55MeV) + SDTL(324MHz, 150 MeV) + OCS(648MHz, 200MeV),
- 6) DTL(324MHz, 70MeV) + SDTL(324MHz, 200 MeV),
- 7) DTL(324MHz, 70MeV) + SDTL(324MHz, 150 MeV) + ACS(972MHz, 200MeV),
- 8) DTL(324MHz, 70MeV) + SDTL(324MHz, 100 MeV) + ACS(972MHz, 200MeV),
- 9) DTL(324MHz, 70MeV) + SDTL(324MHz, 100 MeV) + OCS(648MHz, 200MeV),
- 10) DTL(324MHz, 70MeV) + SDTL(324MHz, 150 MeV) + OCS(648MHz, 200MeV),
- 11) DTL(324MHz, 70MeV) + ACS(972MHz, 200MeV),
- 12) DTL(324MHz, 70MeV) + OCS(648MHz, 200MeV),
- 13) DTL(324MHz, 100MeV) + ACS(972MHz, 200MeV),
- 14) DTL(324MHz, 100MeV) + OCS(648MHz, 200MeV),

- 15) DTL(324MHz, 150MeV) + ACS(972MHz, 200MeV),
- 16) DTL(324MHz, 150MeV) + OCS(648MHz, 200MeV),
- 17) DTL(324MHz, 200MeV).

The possible configurations of the linac complex for an output energy of 400 MeV are as follows:

- 1) DTL(324MHz, 55MeV) + SDTL(324MHz, 200 MeV) + ACS(972MHz, 400MeV),
- 2) DTL(324MHz, 55MeV) + SDTL(324MHz, 150 MeV) + ACS(972MHz, 400MeV),
- 3) DTL(324MHz, 55MeV) + SDTL(324MHz, 100 MeV) + ACS(972MHz, 400MeV),
- 4) DTL(324MHz, 55MeV) + SDTL(324MHz, 100 MeV) + OCS(648MHz, 400MeV),
- 5) DTL(324MHz, 55MeV) + SDTL(324MHz, 150 MeV) + OCS(648MHz, 400MeV),
- 6) DTL(324MHz, 55MeV) + SDTL(324MHz, 200 MeV) + OCS(648MHz, 400MeV),
- 7) DTL(324MHz, 70MeV) + SDTL(324MHz, 200 MeV) + ACS(972MHz, 400MeV),
- 8) DTL(324MHz, 70MeV) + SDTL(324MHz, 150 MeV) + ACS(972MHz, 400MeV),
- 9) DTL(324MHz, 70MeV) + SDTL(324MHz, 100 MeV) + ACS(972MHz, 400MeV),
- 10) DTL(324MHz, 70MeV) + SDTL(324MHz, 100 MeV) + OCS(648MHz, 400MeV),
- 11) DTL(324MHz, 70MeV) + SDTL(324MHz, 150 MeV) + OCS(648MHz, 400MeV),
- 12) DTL(324MHz, 70MeV) + SDTL(324MHz, 200 MeV) + OCS(648MHz, 400MeV),
- 13) DTL(324MHz, 70MeV) + ACS(972MHz, 400MeV),
- 14) DTL(324MHz, 70MeV) + OCS(648MHz, 400MeV),
- 15) DTL(324MHz, 100MeV) + ACS(972MHz, 400MeV),
- 16) DTL(324MHz, 100MeV) + OCS(648MHz, 400MeV),
- 17) DTL(324MHz, 150MeV) + ACS(972MHz, 400MeV),
- 18) DTL(324MHz, 150MeV) + OCS(648MHz, 400MeV).

The effective shunt impedances for each structure used in the calculation are shown in Fig. 10. It is needless to say that we do not think that all of these configurations are realistic, but that the calculated results would be interesting in the sense that how the difference in ZTT among structures influence the main parameters of the linac. The total length and rf power were calculated for each configuration, and are summarized in Tables 5 and 6. A 30-mA beam current was assumed for the beam-power calculation. The accelerating electric fields used in the calculation are shown in Fig. 11. The normalized values by the corresponding Kilpatrick field values (KL) are shown in Fig. 12. The maximum surface electric field is below 1.3 KL for the OCS. They are less than unity for the ACS. The main reason for selecting low fields in the ACS is not a discharge problem, but a decrease in the accelerating efficiency due to a phase slip in the tank. In the simulations described in this section, the same stable phase angle was used for all of the simulations. Therefore, there were beam losses in some of the simulations. In such cases, further improvements are required in order to decrease the beam losses by changing the stable phase angle. Detailed results of the simulations with more realistic structures are given in Table 20 of section 3.9. Figure 13 shows the maximum phase slip in a CCL tank. The effect becomes larger

if the energy is lower and the accelerating field is higher. In our code, the average accelerating fields for both the SDTL and the CCL were determined so that the total power consumption in four successive unit tanks held constant along the linac because of an effective utilization of the klystron power. Thus, the field becomes higher if the shunt impedance is high. Figures 14 and 15 show the variation of the rf driving power along the linac. Therefore, the set of the length and rf power in Tables 5 and 6 is important as a whole. The calculated results are plotted in Fig. 16 for 200-MeV linacs and Fig. 17 for 400-MeV linacs. The optimized configurations for a 400-MeV linac are selected on the assumption that the length is below 205 m, the power is below 56 MW and OCS-II is not included. They are:

2) DTL(324MHz, 55MeV) + SDTL(324MHz, 150 MeV) + ACS(972MHz, 400MeV),

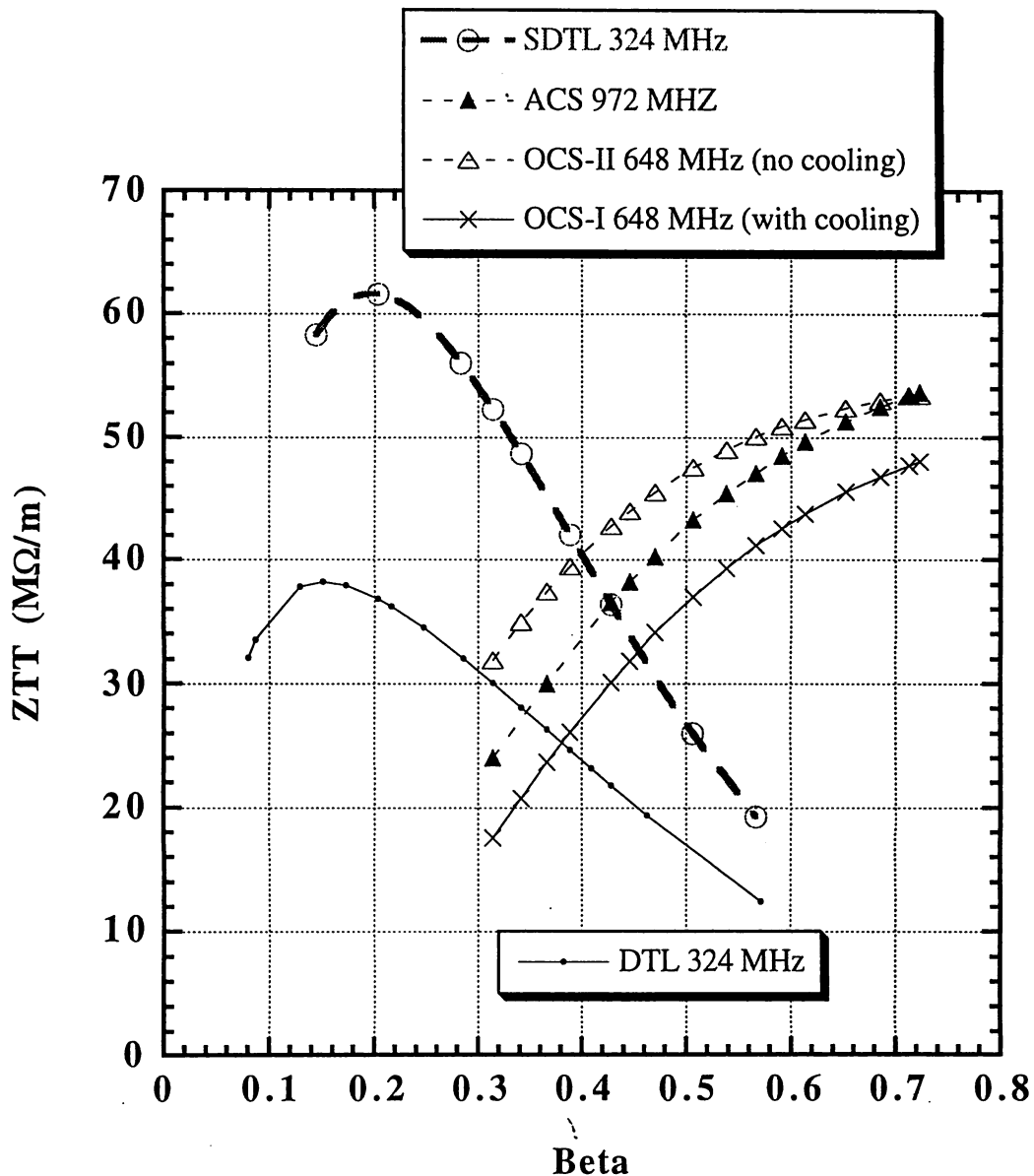


Fig. 10 ZTT vs. beta for various kinds of rf structures. Web thickness, including width of coupling cell, for OCS-I is 28 mm and OCS-II 12 mm. It is 9.5 mm for an ACS.

**Table 5 Summary of the calculated total length and rf power for possible candidates of the linac complex with an output energy of 200 MeV.**

System	Total length m	Total rf power MW
1) DTL(55MeV) + SDTL(200MeV)	116.2	27.1
2) DTL(55MeV) + SDTL(150MeV) + ACS	112.6	27.2
3) DTL(55MeV) + SDTL(100MeV) + ACS	110.9	27.9
4) DTL(55MeV) + SDTL(100MeV) + OCS-I	114.6	29.0
DTL(55MeV) + SDTL(100MeV) + OCS-II	107.7	27.4
5) DTL(55MeV) + SDTL(150MeV) + OCS-I	112.9	27.3
DTL(55MeV) + SDTL(150MeV) + OCS-II	110.5	26.8
6) DTL(70MeV) + SDTL(200MeV)	117.4	27.0
7) DTL(70MeV) + SDTL(150MeV) + ACS	115.0	27.4
8) DTL(70MeV) + SDTL(100MeV) + ACS	113.3	28.0
9) DTL(70MeV) + SDTL(100MeV) + OCS-I	117.0	29.1
DTL(70MeV) + SDTL(100MeV) + OCS-II	110.1	27.5
10) DTL(70MeV) + SDTL(150MeV) + OCS-I	115.3	27.5
DTL(70MeV) + SDTL(150MeV) + OCS-II	112.9	27.0
11) DTL(70MeV) + ACS	121.3	30.7
12) DTL(70MeV) + OCS-I	120.0	30.3
DTL(70MeV) + OCS-II	112.0	28.6
13) DTL(100MeV) + ACS	117.6	28.3
14) DTL(100MeV) + OCS-I	121.3	29.4
DTL(100MeV) + OCS-II	114.4	27.8
15) DTL(150MeV) + ACS	129.7	28.4
16) DTL(150MeV) + OCS-I	130.0	28.5
DTL(150MeV) + OCS-II	127.6	28.0
17) DTL(200MeV)	140.6	28.7

\* A peak current of 30 mA (beam power of 5.9MW) was assumed in the rf power calculation.

\* A drift-length of 0.7 m was assumed for every space between both SDTL and CCL unit tanks.

\* The results are plotted in Fig. 16.

**Table 6 Summary of the calculated total length and rf power for possible candidates of the linac complex with an output energy of 400 MeV.**

System	Total length m	Total rf power MW	CCL Accelerating field MV/m
1) DTL(55MeV) + SDDL(200MeV) + ACS	207.3	55.2	4.3-4.7
2) DTL(55MeV) + SDDL(150MeV) + ACS	201.8	54.5	4.1-4.7
3) DTL(55MeV) + SDDL(100MeV) + ACS	200.2	55.2	3.9-4.7
4) DTL(55MeV) + SDDL(100MeV) + OCS-I	204.6	56.5	3.1-4.0
DTL(55MeV) + SDDL(100MeV) + OCS-II	193.8	54.1	3.8-4.3
5) DTL(55MeV) + SDDL(150MeV) + OCS-I	205.0	55.5	3.4-4.0
DTL(55MeV) + SDDL(150MeV) + OCS-II	196.6	53.5	4.0-4.3
6) DTL(55MeV) + SDDL(200MeV) + OCS-I	211.7	56.4	3.6-4.0
DTL(55MeV) + SDDL(200MeV) + OCS-II	206.2	55.2	4.1-4.3
7) DTL(70MeV) + SDDL(200MeV) + ACS	208.5	55.1	4.3-4.7
8) DTL(70MeV) + SDDL(150MeV) + ACS	204.2	54.7	4.1-4.7
9) DTL(70MeV) + SDDL(100MeV) + ACS	202.6	55.3	3.9-4.7
10) DTL(70MeV) + SDDL(100MeV) + OCS-I	207.0	56.6	3.1-4.0
DTL(70MeV) + SDDL(100MeV) + OCS-II	196.2	54.2	3.8-4.3
11) DTL(70MeV) + SDDL(150MeV) + OCS-I	207.4	55.7	3.4-4.0
DTL(70MeV) + SDDL(150MeV) + OCS-II	199.0	53.7	4.0-4.3
12) DTL(70MeV) + SDDL(200MeV) + OCS-I	212.9	56.4	3.6-4.0
DTL(55MeV) + SDDL(200MeV) + OCS-II	207.4	55.2	4.1-4.3
13) DTL(70MeV) + ACS	208.6	57.5	3.6-4.7
14) DTL(70MeV) + OCS-I	214.3	59.1	2.8-4.0
DTL(70MeV) + OCS-II	198.1	55.3	3.6-4.3
15) DTL(100MeV) + ACS	206.9	55.6	3.9-4.7
16) DTL(100MeV) + OCS-I	211.3	56.9	3.1-4.0
DTL(100MeV) + OCS-II	200.5	54.5	3.8-4.3
17) DTL(150MeV) + ACS	218.9	55.7	4.1-4.7
18) DTL(150MeV) + OCS-I	222.1	56.7	3.4-4.0
DTL(150MeV) + OCS-II	213.7	54.7	4.0-4.3

\* A peak current of 30 mA (beam power of 11.9MW) was assumed in the rf power calculation.

\* A drift-length of 0.7 m was assumed for every space between both SDDL and CCL unit tanks.

\* The results are plotted in Fig. 17.

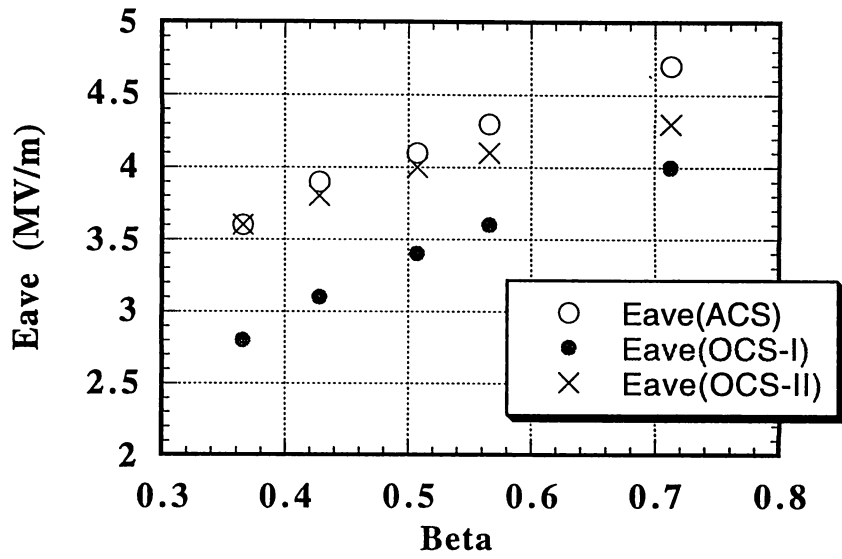


Fig. 11 Average accelerating field used in the calculation for three kinds of structures.

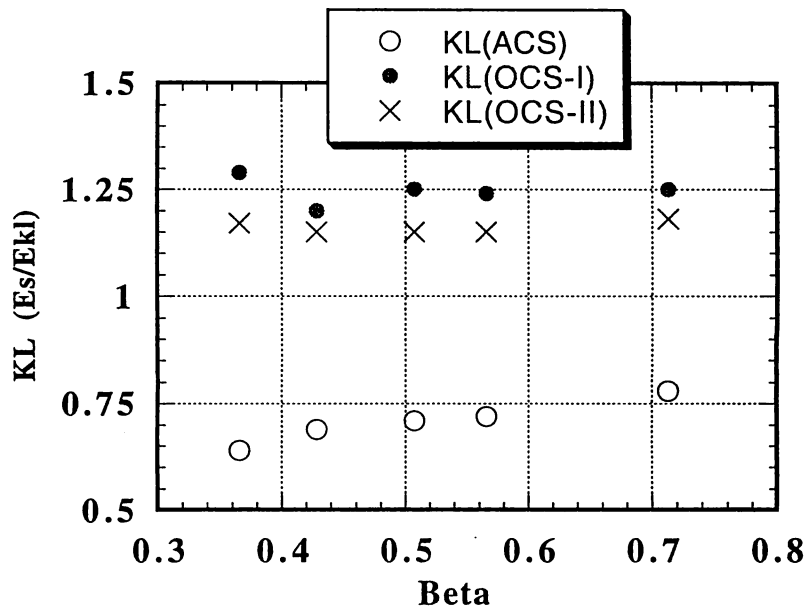


Fig. 12 Average accelerating field normalized by the corresponding Kilpatrick field limit for three kinds of structures.

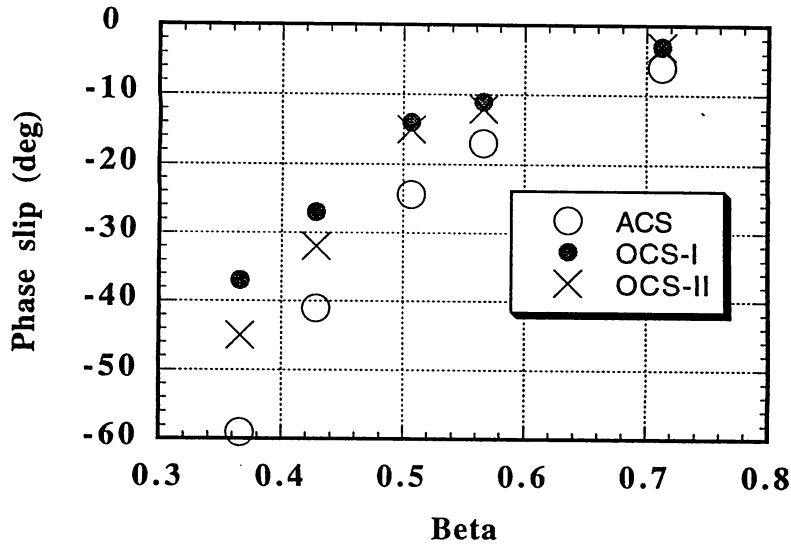


Fig. 13 Phase slip in a unit tank for three kinds of structures.

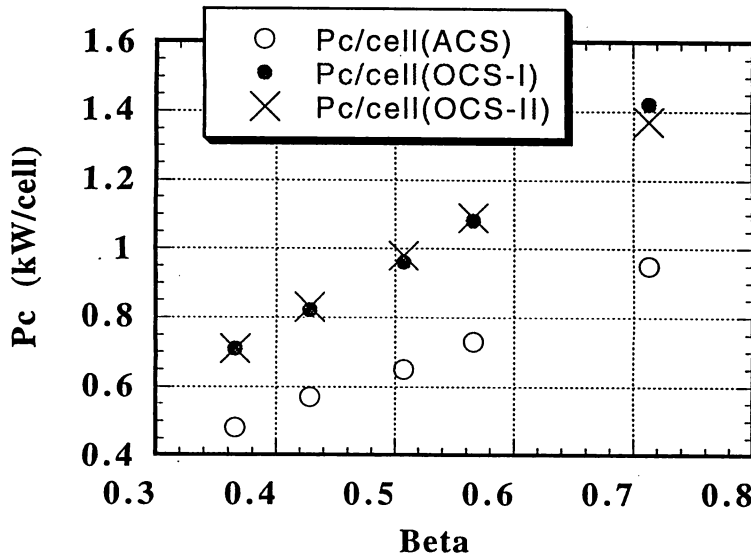


Fig. 14 Rf driving power per cell in the calculation for three kinds of structures.

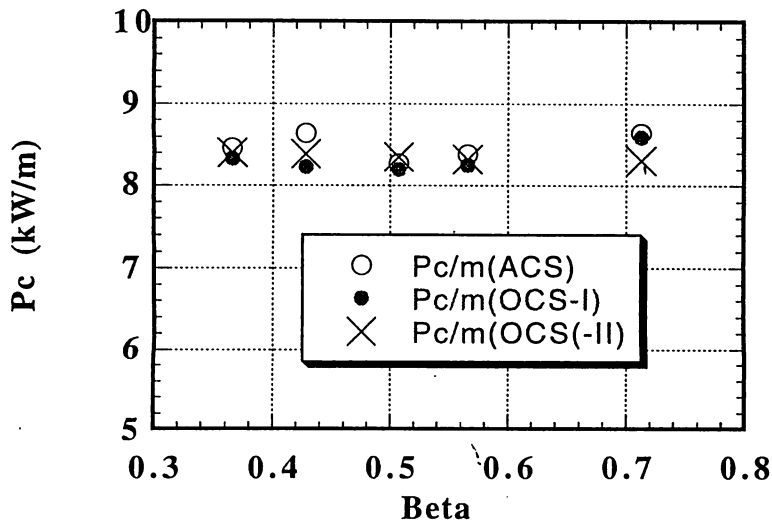


Fig. 15 Rf driving power per unit length in the calculation for three kinds of structures.

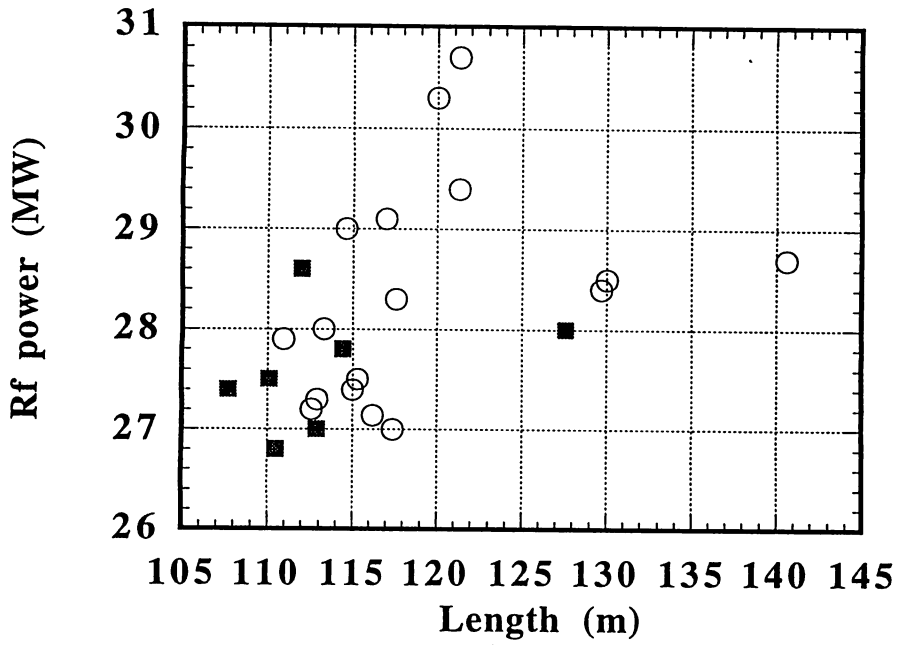


Fig. 16 Total required rf power vs. total required length for all configuration of the 200-MeV linac given in Table 5. The square points indicate the configurations with OCS-II.

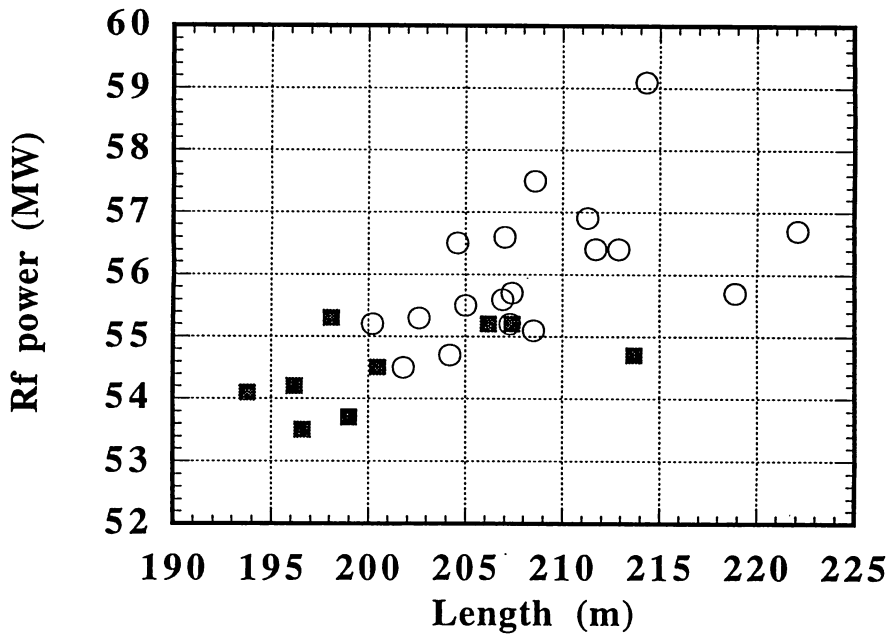


Fig. 17 Total required rf power vs. total required length for all configuration of the 400-MeV linac given in Table 6. The square points indicate the configurations with OCS-II.

- 3) DTL(324MHz, 55MeV) + SDTL(324MHz, 100 MeV) + ACS(972MHz, 400MeV),
- 8) DTL(324MHz, 70MeV) + SDTL(324MHz, 150 MeV) + ACS(972MHz, 400MeV),
- 9) DTL(324MHz, 70MeV) + SDTL(324MHz, 100 MeV) + ACS(972MHz, 400MeV).

They seem to be reasonable results judging from their ZTT given in Fig. 10. The selected four configurations also show good performance for a 200-MeV linac. It seems that the differences among them are not large. Thus, all of them are a good solution for the JHP linac configuration from the view point of ZTT-optimization. Here, the OCS-II structure is excluded, since the lack of a water channel for cooling the nose-corn part does not seem to be realistic for the JHP high-duty factor linac. In fact, an average rf power of more than 8 kW/m is required in order to make the linac-length around 200 m. Such high power operations have a possibility of a serious deformation of the cavity, due to a rise in the temperature of the inner surface.

The OCS-II structure is dismissed because of a heat problem during operation.  
The OCS-I structure is also dismissed because of its low efficiency in the low- $\beta$  region.

Finally, it is pointed out that the following corrections are required for comparing the rf driving power with those given in other literature:

- 1) subtract the beam power from the total rf power,
- 2) divide by a factor of 1.2 - 1.3 in order to obtain the idealized value, since our rf driving power already includes a factor of 1.3 for the DTL and 1.2 for both the SDTL and CCL.

For example, the DTL (200 MeV, No. 17 in Table 5) is 140.6 m in total length and 28.7 MW in total rf power. Remembering that the beam power is 5.9 MW for a 30-mA beam and taking into account the rf multiplying factor of 1.3 and the drift spaces between unit tanks, the length for the total tank becomes 130.2 m and the rf driving power is 17.5 MW.

### 3.7 DTL design

#### 3.7.1 DTL focusing design

Both the transverse and longitudinal focusing parameters are determined on the basis of equipartitioning theory combined with coupled envelope equations for the bunched beam, written as (ref. 8):

$$k_{x0a}^2 - \frac{3}{2} \frac{Nr_c}{\beta_0^2 \gamma_0^3} \frac{1}{az_m} \left( 1 - \frac{g_0}{2} \frac{a^2}{\gamma_0^2 z_m^2} \right) - \frac{\epsilon_{nx}^2}{\beta_0^2 \gamma_0^2 a^3} = 0,$$

$$k_{z0z_m}^2 - \frac{3}{2} \frac{Nr_c}{\beta_0^2 \gamma_0^5} \frac{g_0}{z_m^2} - \frac{\epsilon_{nz}^2}{\beta_0^2 \gamma_0^6 z_m^3} = 0,$$

$$r_c = \frac{q^2}{4\pi\epsilon_0 mc^2},$$

$$g_0 = 2 \frac{z_m^2}{a^2} M_x.$$

Here,  $k_{x0}$  and  $k_{z0}$  are the zero-current wave numbers for transverse and longitudinal oscillations,  $\epsilon_x$  and  $\epsilon_z$  the rms emittances of the transverse and longitudinal phase spaces,  $a$  and  $z_m$  the radii of the bunch in the transverse and longitudinal directions,  $N$  the number of particles in a bunch,  $M_x$  the ellipsoidal form factor,  $q$  the unit charge,  $\epsilon_0$  the vacuum permeability,  $c$  the velocity of light,  $\beta_0$  the relative velocity and  $\gamma_0$  the relativistic parameter. The wave numbers, including space-charge effects, are written as

$$k_x^2 = k_{x0}^2 - \frac{3}{2} \frac{Nr_c}{\beta_0^2 \gamma_0^3} \frac{1}{a^2 z_m} \left( 1 - \frac{g_0}{2} \frac{a^2}{\gamma_0^2 z_m^2} \right).$$

$$k_z^2 = k_{z0}^2 - \frac{3}{2} \frac{Nr_c}{\beta_0^2 \gamma_0^5} \frac{g_0}{z_m^3}.$$

Therefore, the focusing parameters as well as the beam parameters should be calculated cell by cell using the initial parameters given at the entrance of the linac.

In general, the distribution of the accelerating field within a tank remains uniform, since it is not easy to vary the field distribution without any troublesome reactions during operation. Therefore, the longitudinal focusing strength ( $k_{z0}$ ) is fixed during operation, and varies as the energy increases,

$$k_{z0} \propto \frac{1}{(\beta_0 \gamma_0)^{3/2}}.$$

On the contrary, the transverse focusing force varies as

$$k_{x0} \propto \frac{1}{\beta_0}$$

if the zero-current phase advance remains constant along the acceleration. One choice of the variation of the focusing forces is to keep the ratio between the transverse and longitudinal focusing forces constant along the acceleration. In such a case, the transverse focusing force should be decreased along the acceleration in the same manner as the longitudinal force. Then, the transverse beam radius becomes larger than that with the constant phase-advance focusing method. It is also a good choice from the viewpoint of space-charge effects, since the density of the bunch decreases. A demerit of this focusing method is that it requires a larger bore radius.

The injection parameters, related to both the beams and structures, are chosen so that the equipartitioning condition is satisfied. The condition is given by

$$\gamma_0 \frac{\epsilon_{nx}}{\epsilon_{nz}} \frac{z_m}{a} = 1 \quad \text{or} \quad \frac{k_x \epsilon_{nx}}{k_z \epsilon_{nz}} = 1,$$

where the suffix of  $n$  means a normalized emittance and  $k_x$  and  $k_z$  are the wave numbers of the transverse and longitudinal phase oscillations with space-charge. It is noted that the injection parameters are closely related to the focusing parameters along the acceleration. Therefore, if the equipartitioning condition can not be fulfilled adequately, it is possible to control the emittances during acceleration. Matched and equipartitioned parameters of the injection beam into the DTL are listed in Table 7. The main focusing parameters along the DTL are plotted in Figs. 18, 19 and 20. These parameters are typical. In the operation, the focusing parameters should be calculated again according to both the measured injection beam parameters and the focusing design along the DTL. Details of the focusing design will be reported elsewhere.

The unit-tank length of the DTL relates to the peak output power from a klystron. Table 8 gives the main parameters of the DTL design. A klystron with a 3-MW output power is desirable for the following two reasons:

- 1) a smaller number of DTL tanks and rf systems generally means less cost and easier tuning, and
- 2) a smaller number of drift space between the DTL tank is more desirable from the viewpoint of longitudinal motion.

However, an increase in the peak power requires more severe requirement for the rf components, resulting in a higher cost and a higher possibility of failure.

### **3.7.2 Transition energy from the DTL to the SDTL**

The transition energy from the DTL to the SDTL is discussed from the following viewpoints:

- 1) the longitudinal beam quality at the exit (200 MeV),
- 2) the transverse beam quality at the exit (200 MeV),
- 3) ZTT optimization of the total system of the DTL and the SDTL and
- 4) rf and mechanical structure issues related to the unit tank length.

A higher transition energy is favorable from the viewpoints of items (1) and (4), since the effects of the drift spaces on the beam quality generally decrease as the energy increases and the longitudinal dimension of the SDTL structure increases, provided that a fixed number of unit cells is chosen for a unit tank throughout the SDTL section. There is a rotation of the longitudinal emittance in phase space along the acceleration. The effects of the drift space between the DTL and the SDTL depends upon both the shape of the longitudinal emittance at the exit of the structure and the strength of the space-charge effects. Therefore, the optimum energies for the transition should be determined based on the calculated final beam quality at the exit of the linac.

**Table 7 Matched and equipartitioned parameters of the injection beam into the DTL.**

Current	30	60	mA
Beam radius (90%)	1.83	1.98	mm
Beam radius (rms)	0.82	0.89	mm
$\Delta p/p$ (rms)	0.004	0.004	
$\Delta\phi$ (rms)	7.7	9.1	degree
Bunch length (rms)	1.6	1.9	mm
Bunch length (90%)	3.5	4.2	mm
$\epsilon_{nx}$ (90%)	1.5	1.5	$\pi$ mm-mrad
$\epsilon_{nz}$ (90%)	2.5	3.0	$\times 10^{-6}$ m
B'	107.4	107.4	T/m
$\sigma_{x0}$	58	58	degree
$\sigma_x$	48	42.7	degree
$\sigma_{z0}$	30	30	degree
$\sigma_z$	21.5	18.1	degree
$\Delta w$ (rms, half)	24	24	keV
$\Delta w$ (90%,half)	53.7	53.7	keV
$\Delta\phi$ (90%,half)	17.2	20.3	degree
Partition parameter	1.15	1.06	

**Table 8 Main parameters of the DTL linac.**

Tank number	1	2	3	Sum	
$W_{in}$	3.0	19.20	35.41		MeV
$W_{out}$	19.20	35.41	50.1		MeV
Pc	1.16	1.36	1.40	3.92	MW
$P_b(30mA)$	0.49	0.49	0.44	1.41	MW
$P_b(60mA)$	0.97	0.97	0.88	2.82	MW
$P_{tot}(30mA)$	1.64	1.84	1.84	5.33	MW
$P_{tot}(60mA)$	2.08	2.33	2.28	6.74	MW
Tank length	10.36	8.87	7.81	28.51	m
Number of cells	80	41	29	150	
Accelerating field	2.5	2.7	2.9		MV/m
Drift space	0.74	0.74			m

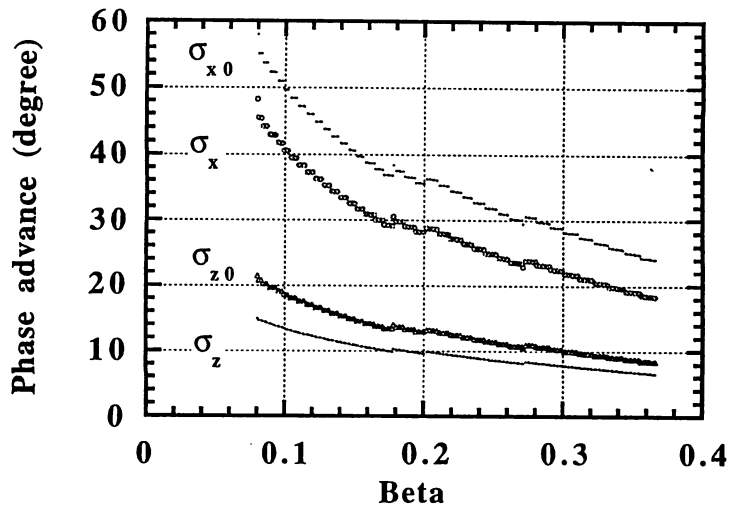


Fig. 18 Phase advances in both the transverse and longitudinal phase spaces along the DTL. A peak current of 30 mA is assumed.

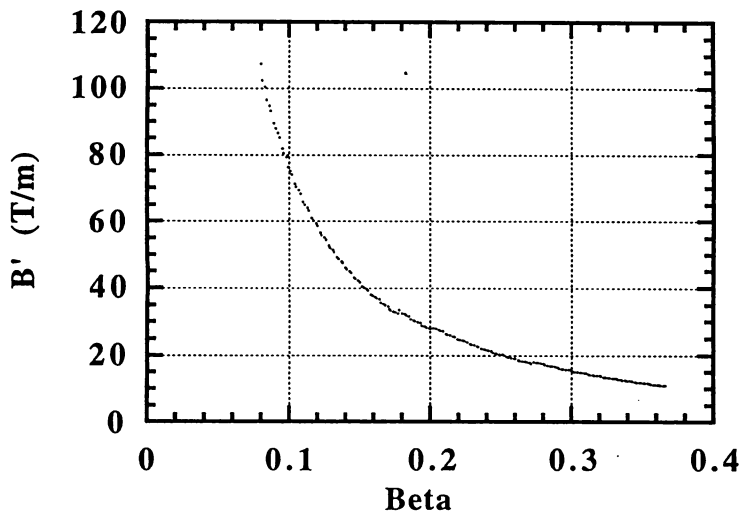


Fig. 19 Required magnetic field gradient along the DTL.

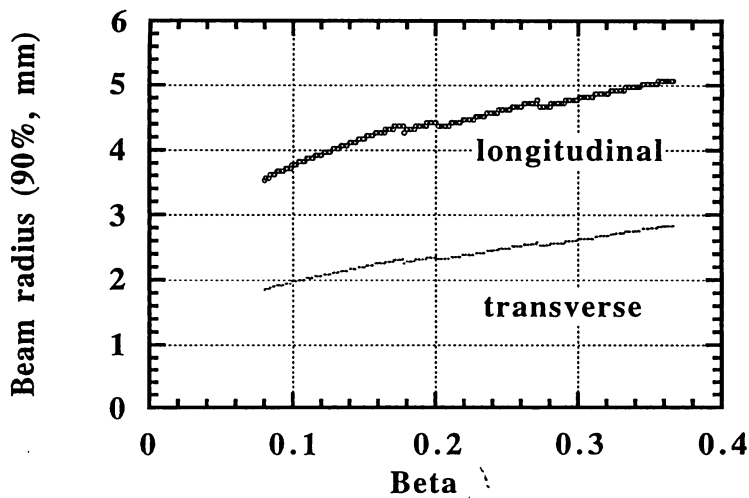


Fig. 20 Variation of the beam size along the DTL.

A lower transition energy is desirable from the viewpoint of items (2) and (3). Since the transverse beam size in the SDTL is larger than that in the DTL, the space-charge effects can be reduced in the SDTL. It is clear from Fig. 10 that a lower transition energy is desirable from the viewpoint of ZTT optimization. Therefore, a compromise is required for this issue.

A calculation through the DTL structure was performed by the code PARMILA using a six-dimensional matched 30-mA beam. There is a 1.4-m long drift space for beam matching between the DTL and the SDTL. Two kinds of matching were performed: one was matching only in the transverse motion (XY-matching), and the other was matching in both the transverse and longitudinal motions (XYZ-matching). Then, the beam is injected into the SDTL. The rms width of the output energy at the exit of the SDTL (200 MeV) as a function of various injection energies into the SDTL are shown in Fig. 21. Judging from these simulations, our conclusions are as follows:

- 1) a large oscillation of the energy spread in the SDTL is seen in the case of only transverse matching,
- 2) the minimum energy spreads in the transverse-matching simulation are nearly the same as those in the both-matching simulation,
- 3) there are a few optimum points which correspond to the bottom of the energy oscillation at the exit of the SDTL: about 37, 50 and 65 MeV.
- 4) the amplitude of the energy oscillation decreases as the transition energy increases,
- 5) a longitudinal matching device is not necessary if the optimum output energy from the DTL is selected.

Fixing the injection energy into the SDTL at 50.0 MeV, the injection phase dependence of the beam quality from the SDTL was studied using the injection beam into the DTL given in Table 9. Here, only transverse matching was performed. The results are shown in Figs. 22 and 23. It can be seen that a satisfactory wide phase acceptance was obtained. The energy width of the output beam depends upon the injection phase as a result of filamentation in the longitudinal phase space. In both figures,  $\phi_{in}$  denotes the deviation from the stable phase angle at the injection point.

The main parameters are summarized in Table 9. The results of acceleration by all DTL configurations are also shown. In conclusion, there is some degradation in the beam quality in SDTL acceleration compared with that in all DTL configuration; however, it is so small that it is allowable for our design requirements.

### 3.7.3 LINSAC simulation for the DTL and the SDTL

In the work mentioned in the previous section, the modified PARMILA code was used in order to study the general features of the systems. In order to study the details of the configuration, the code LINSAC (ref. 9) was used for both the DTL and the SDTL acceleration. Here, four

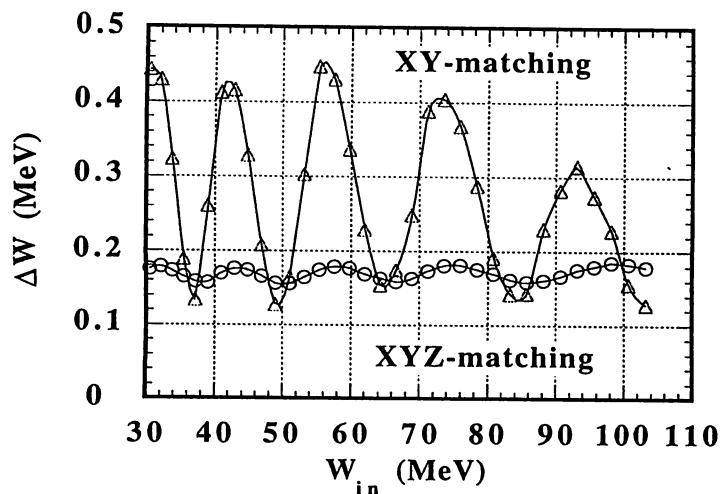


Fig. 21 Energy-width of the SDTL output beam as a function of the injection energy.

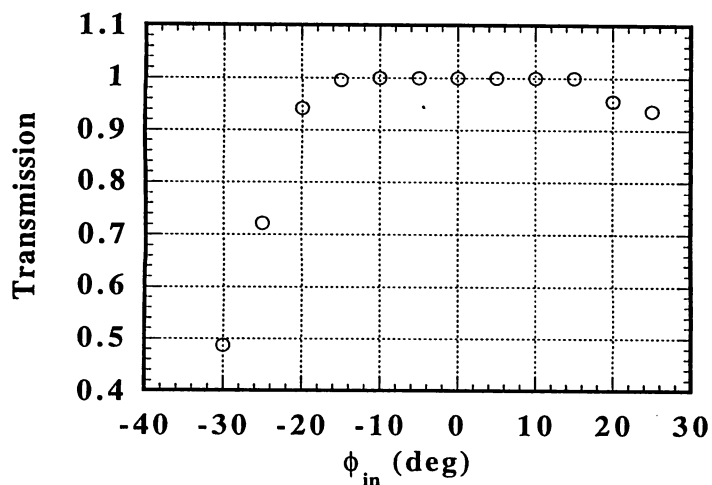


Fig. 22 Transmission ratio through the SDTL as a function of the injection phase. An injection energy of 50.0 MeV is used.

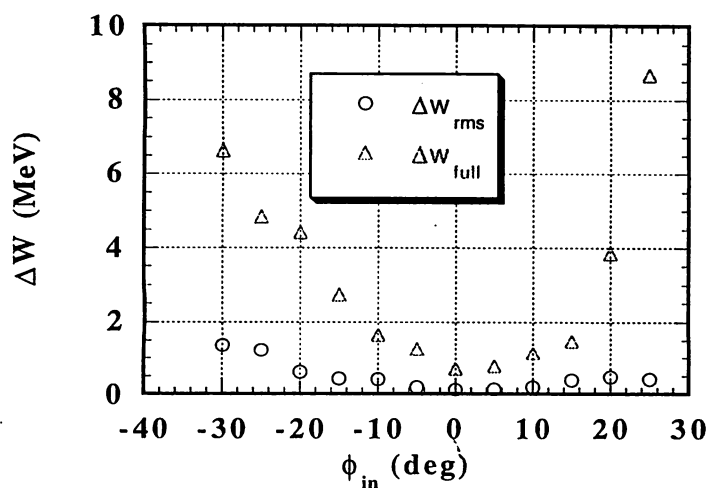


Fig. 23 Energy-width of the SDTL output beam as a function of the injection phase. An injection energy of 50.0 MeV is used.

acceleration configurations up to an energy of 200 MeV (Type-1, Type-2, Type-3 and all DTL) are considered, as listed in Table 10. The Type-1 uses two tanks for the DTL section, Type-2 uses three tanks and Type-3 uses four tanks for the DTL section. The accelerating field used in these simulations were low (2.5 MV/m) compared with those mentioned in the previous section. However, this did not cause any important difference in the calculated results. The three injection energies into the SDTL were 32.2, 47.3 and 62.1 MeV, which were determined by the rf power limit of the klystrons for each DTL tank. Therefore, the injection energies were not the optimum values in the sense that they corresponded to the bottom of the oscillation of the energy width of the output beam at the 200-MeV exit, which was discussed in the previous section. However, these kinds of miss-matchings can possibly occur if the shape of the longitudinal emittance is different from that in the optimum calculation. The number of macro-particles was 3200 in the simulation.

The total systems combined with the SDTL sections are summarized in Table 11. Transverse matching was performed before injection into the SDTL structure. A 20-mA beam was assumed in these simulations. The results of the simulation are summarized in Table 12. The standard simulation is 'DTL-out-1', in which there are no drift spaces between adjacent unit DTL tanks. This gives the most superior longitudinal beam quality after acceleration up to 200 MeV. Next, the simulation of 'DTL-out-2' shows a slight increase (20%) in the longitudinal emittances due to the effects of drift spaces of less than 1 m between the DTL tanks. It is of interest that the transverse emittances are smaller than those in 'DTL-out-1'. Three combined configurations (Type-1, 2 and 3) give larger transverse emittances than those in all DTL configuration. As for the longitudinal emittances, interpreting the results becomes complicated, since there are two main reasons for increasing the longitudinal emittances: the shape of the

**Table 9 Comparison of the main parameters between (DTL+SDTL) and all DTL configuration. The output energy is 200 MeV. The code PARMILA was used for the SDTL simulations.**

	DTL + SDTL	all DTL	Input beam	
	rms/90%	rms/90%	rms/90%	
$\epsilon_x$	0.453/2.06	0.427/1.86	0.374/1.58	$\pi$ mm-mrad
$\epsilon_y$	0.519/2.42	0.435/1.89	0.373/1.57	$\pi$ mm-mrad
$\epsilon_z$	0.335/1.30	0.302/1.21	0.263/1.12	$\pi$ MeV-deg
$\Delta w_{rms}$	0.150	0.160	0.029	MeV
$\Delta w_{90\%full}$	0.480	0.520	0.129	MeV
Length(cavity)	93.0	128.7 m	$\Delta\phi_{rms}=9.4$	degree
Total length	121.0	139.0 m	$\Delta\phi_{90\%full}=42.0$	degree
Pc	17.5	14.48 MW		

\* Pc does not include other loss factors.

\* The increase in Pc for SDTL structure is due to its high field gradient.

\* The injection particles of 2000 are generated at the entrance of the DTL.

**Table 10 Parameters of the DTL part of 200-MeV linac for the LINSAC simulation.**

No	ENERGY 3 MeV	CELL	LENGTH cm	Pc MW	Pb MW	Ptot MW	DRIFT cm
1	16.353	69	843.787	0.827	0.401	1.228	68.2
2	32.154	45	917.051	1.039	0.474	1.513	70.9
3	47.274	33	857.888	1.025	0.454	1.479	84.9
4	62.118	27	816.131	1.165	0.445	1.610	

**Table 11 Parameters of the combined 200-MeV linac for the LINSAC simulation.**

	Type-1	Type-2	Type-3	All DTL	
DTL energy	3-32	3-47	3-62	3-200	MeV
DTL tank number	2	3	4	18	
DTL length	18.29	27.58	36.59	143.58	m
DTL cell	114	147	174	395	
DTL Pc	1.87	2.89	4.06	18.66	MW
DTL Pbeam	0.88	1.33	1.77	5.92	MW
DTL total power	2.74	4.22	5.83	24.58	MW
SDTL tank No.	46	42	38		
SDTL length	135.43	128.58	116.89		m
SDTL cell	243	224	192		
SDTL Pc	14.58	13.93	12.67		MW
SDTL Pbeam	5.04	4.58	4.14		MW
SDTL total power	19.62	18.51	16.81		MW
Total length	153.72	156.16	153.48	143.58	m
Total rf power	22.36	22.73	22.64	24.58	MW

**Table 12 Output emittances of the DTL-SDTL simulations by the code LINSAC.**

	$\epsilon_x(\text{rms})$	$\epsilon_x(90)$	$\epsilon_y(\text{rms})$	$\epsilon_y(90)$	$\epsilon_z(\text{rms})$	$\epsilon_z(90)$	
	$\pi$ mm-mrad		$\pi$ MeV-deg				
Type-1	0.596	2.61	0.667	3.17	0.384	1.70	
Type-2	0.561	2.50	0.677	3.06	0.484	2.53	
Type-3	0.564	2.47	0.586	2.74	0.413	2.06	
DTL out-1	0.439	2.02	0.429	2.04	0.330	1.40	all DTL without drift spaces
DTL out-2	0.417	1.89	0.409	1.81	0.418	1.90	all DTL with drift spaces

longitudinal emittance from the DTL and the space-charge effect. In connection with these points, an increase in the longitudinal emittance due to the drift space between the DTL and the SDTL is shown in Fig. 24. The results were normalized by that without a drift space. This suggests more clearly that both a shorter drift space between the DTL and SDTL and a higher transition energy are desirable from the viewpoint of decreasing the effects of the drift space between the DTL and the SDTL.

Two important points should be pointed out in connection with the LINSAC simulations in this section:

- 1) the number of macro-particles used in the simulation was rather small. Therefore, a larger emittance growth ratio is expected, as shown in section 3.8.4,
- 2) the focusing magnets are placed on both end plates of the SDTL tank because of the requirement of a higher ratio of vectorization of the code, which is different from those of the real structures.

Thus, a comparison among the results for different kinds of simulations within the section seems to be useful; however, it seems to be difficult to compare the absolute values of each simulation with the other results of the simulation in other sections.

### **3.7.4 SDTL simulation with rf field errors**

In real acceleration there are inevitably rf field errors in an accelerator structure, both rf amplitude and phase. Thus, the effects of field errors in the SDTL acceleration are estimated by using a modified PARMILA code. Here, the injection of 10000 macro-particles into the SDTL was produced by the LINSAC code for the DTL structure with the more realistic beam emittances given in Table 15 of section 3.8.3.

The beam from the DTL travels a 1.4-m long drift space and is injected into the SDTL with transverse matching. There are two kinds of field errors. One is errors for each cell. The other is errors for each tank. The errors for each kind are randomly produced in the uniform distribution. The simulation results are plotted from Figs. 25 - 29. Several results are pointed out:

- 1) the longitudinal emittances as well as the energy spread increases as the field errors,
- 2) the beam loss increases as the field errors, which gives tolerances for the field errors,
- 3) the transverse emittances do not change much.

If we set the limit of the beam loss below 0.1 - 0.2%, the allowable amplitude error for each cell is  $\pm 1\%$ , for each tank  $\pm 3\%$  and the phase error for each tank  $\pm 4\%$ . The phase errors for each cell within a unit tank can be set zero for the SDTL structure. It should be pointed out that these limits depend upon the properties of the injected beam.

## **3.8 Beam simulation for studying the transition from the DTL/SDTL to the CCL**

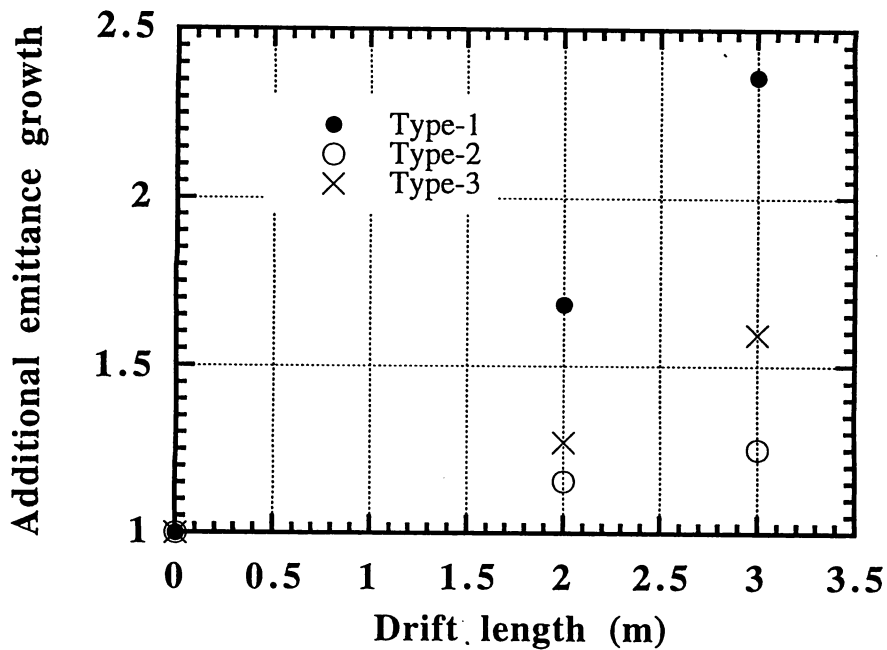


Fig. 24 Additional longitudinal emittance growth due to the drift space between the DTL and the SDTL. The results are normalized by those without a drift space.

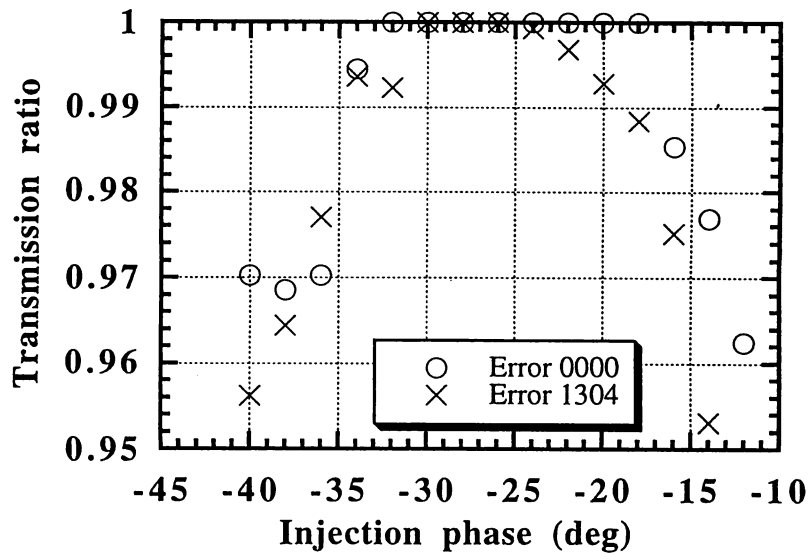


Fig. 25 Effects of field errors on the transmission ratio of the SDTL output beam versus the injection phase. 'Error 1304' means amplitude errors of 1% for each cell, 3% for each tank, phase errors of 0% for each cell and 4% for each tank.

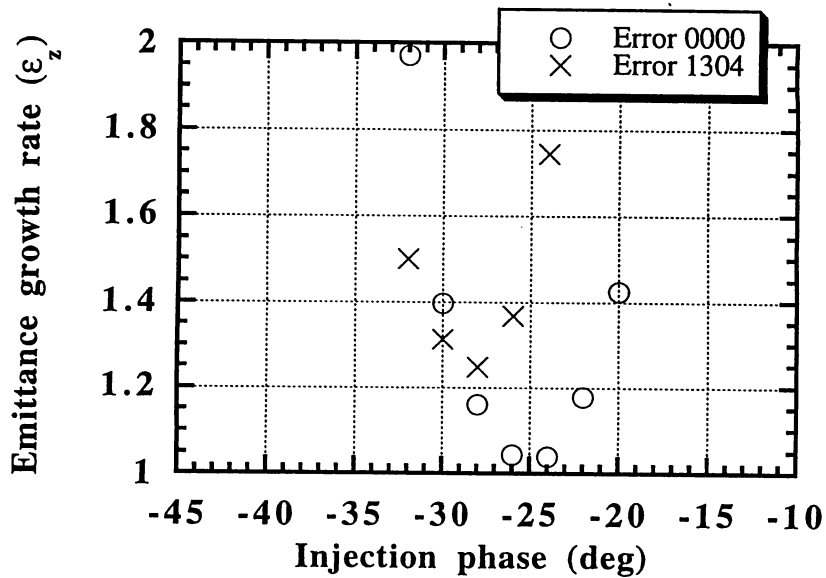


Fig. 26 Effects of field errors on the longitudinal emittance of the SDTL output beam versus the injection phase. 'Error 1304' means amplitude errors of 1% for each cell, 3% for each tank and phase errors of 0% for each cell and 4% for each tank.

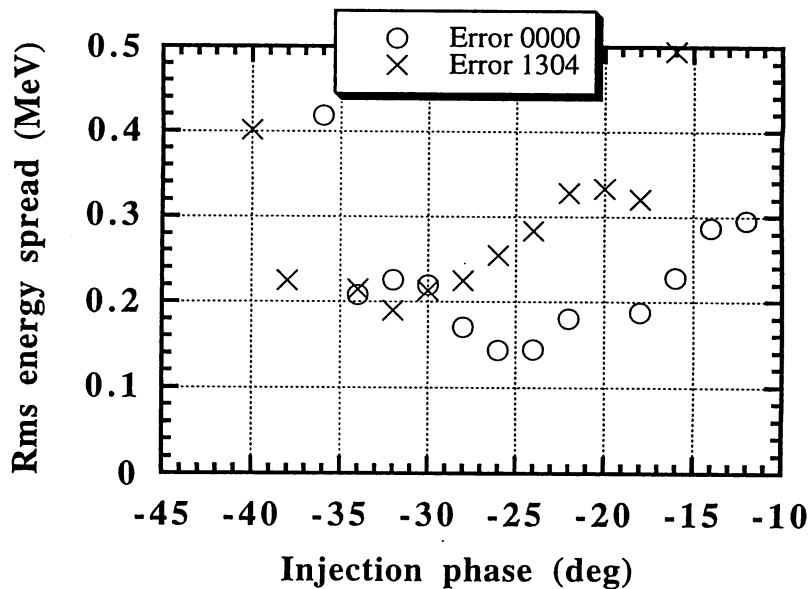


Fig. 27 Effects of field errors on the rms energy spread of the SDTL output beam versus the injection phase. 'Error 1304' means amplitude errors of 1% for each cell, 3% for each tank and phase errors of 0% for each cell and 4% for each tank.

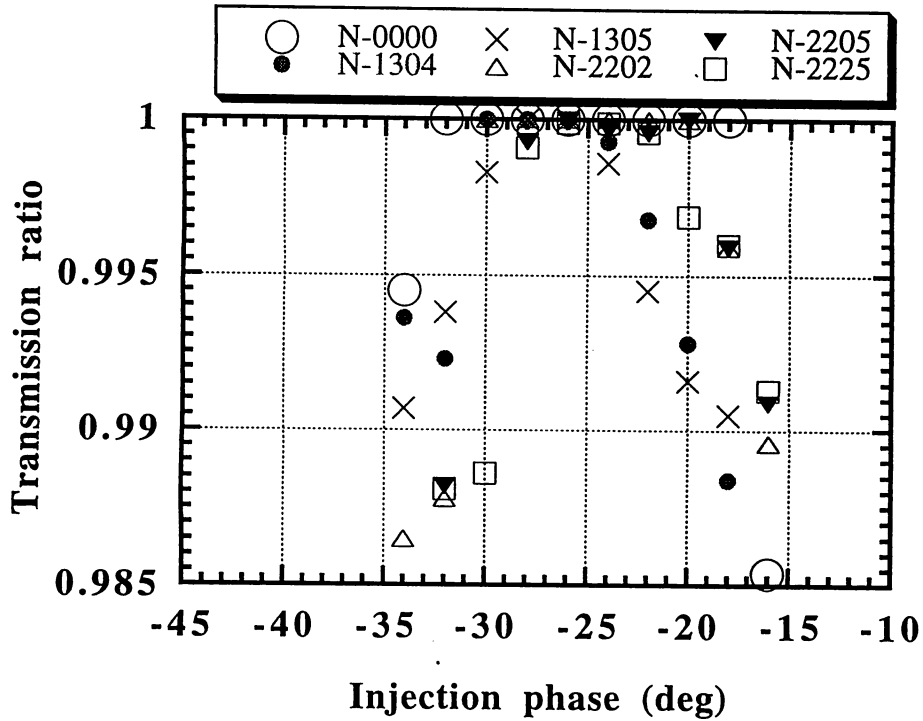


Fig. 28 Effects of field errors on the transmission ratio of the SDTL output beam versus the injection phase for various types of errors. 'Error 1304' means amplitude errors of 1% for each cell, 3% for each tank and phase errors of 0% for each cell and 4% for each tank.

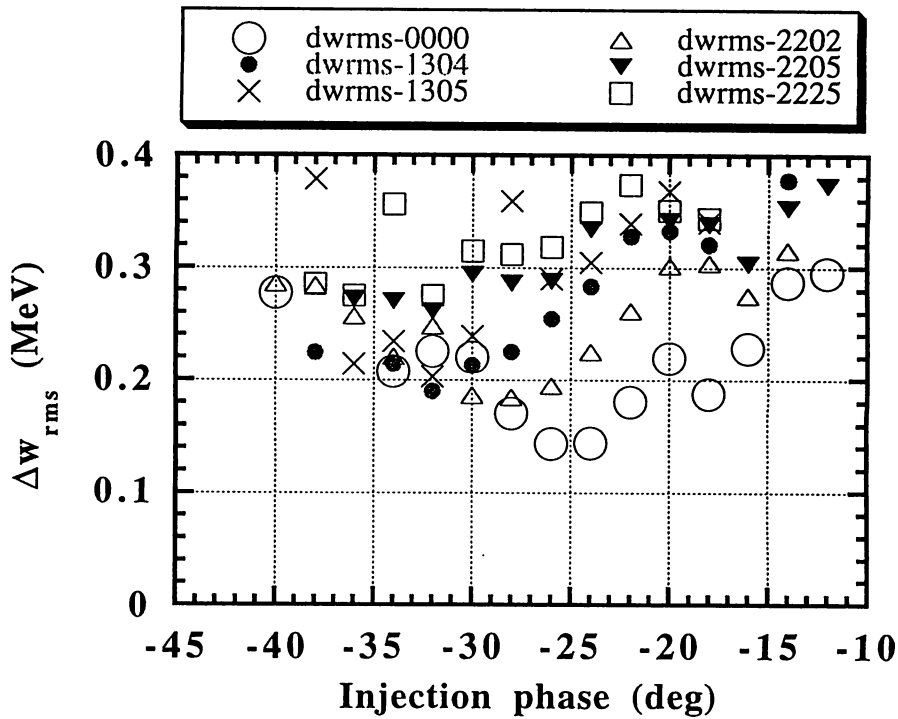


Fig. 29 Effects of field errors on the rms energy spread of the SDTL output beam versus the injection phase for various types of errors. 'Error 1304' means amplitude errors of 1% for each cell, 3% for each tank and phase errors of 0% for each cell and 4% for each tank.

Beam simulations were performed in order to study the effects of transition from the DTL to the CCL upon the output beam quality. Two CCL frequencies (972 and 1296 MHz) and two transition energies (100 and 147 MeV) were considered. The output beam from the DTL, calculated with the code LINSAC, was transformed so as to match with the acceptances of the CCL. A 2-m long drift space between the DTL and the CCL was assumed. The following four configurations were studied:

- 1) DTL-100 MeV + 972-MHz CCL,
- 2) DTL-100 MeV + 1296-MHz CCL,
- 3) DTL-147 MeV + 972-MHz CCL and
- 4) DTL-147 MeV + 1296-MHz CCL.

Acceleration was performed up to 400 MeV by using the code PROEND, which calculated the beam motion in a  $\pi/2$  mode structure using a similar method to that in the code PARMILA.

In order to study the configurations of the linac, some assumptions were required for obtaining meaningful results. One method was to use the optimized parameters from the viewpoint of the beam-dynamics behavior for each configuration. However, this scheme had some possibility of sacrificing or screening technical problems or construction cost. The other was to adjust one accelerating property for all configurations. Here, the following assumptions were applied for comparing the calculated results for the different configurations of the linac:

- 1) the tank length was determined so that the transverse acceptance would be approximately equal for all configurations,
- 2) the accelerating field was determined so that the sum of the rf power of successive four tank would be nearly equal,
- 3) the drift space between two adjacent unit tanks was nearly equal for all configurations,
- 4) the injection beam into the DTL was chosen as being nearly similar to the result of the RFQ calculation,
- 5) the code LINSAC accelerated a beam of 10000 macro-particles from 3 MeV to 100 and 147 MeV, which was used as the injection beam into the CCL,
- 6) a beam current of 30 mA was assumed in the code LINSAC.

### 3.8.1 Transmission

Figures 30 and 31 show the transmission ratio for each configuration as a function of the injection phase into the CCL structure. The following items are pointed out:

- 1) a frequency multiplication factor (FMF) of three can be allowed at an energy range of 150 MeV. If a transition energy of 100 MeV is selected, combined with an FMF of three, more effort would be required in order to achieve no-beam loss acceleration,

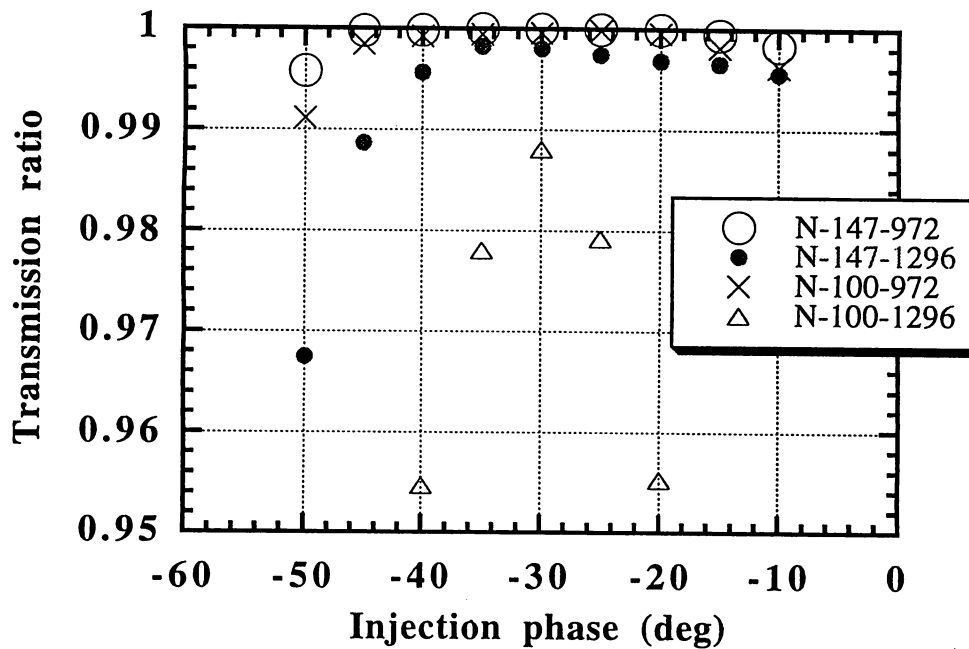


Fig. 30 Transmission ratio through the CCL as a function of an injection phase for four configurations of the linac. No field errors are assumed. The number of particles is 10000. The notation 'N-147-972' means an injection energy of 147 MeV and a frequency of 972 MHz.

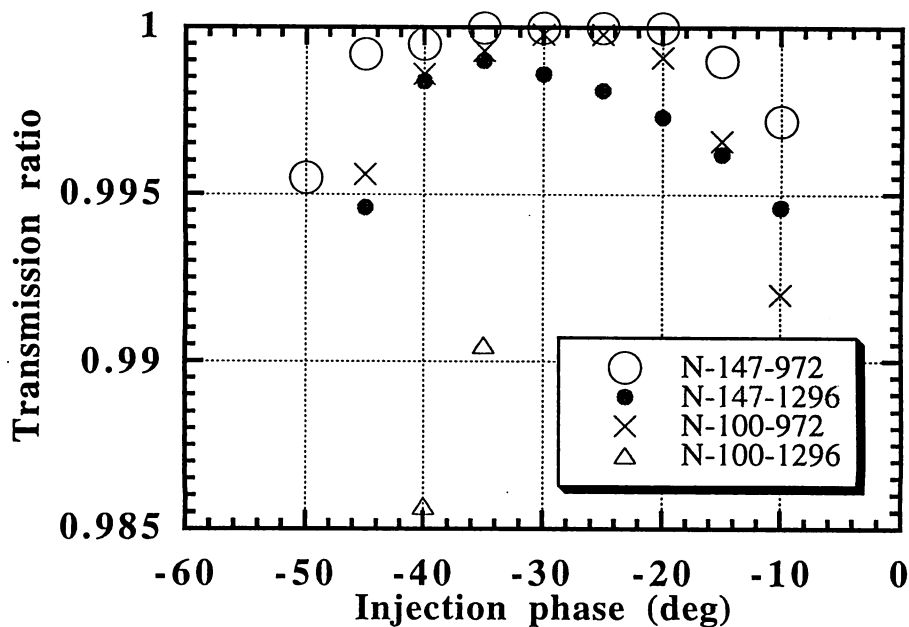


Fig. 31 Transmission ratio through the CCL as a function of the injection phase for four configurations of the linac. Rf amplitude errors of 1% for each cell and 3% for each tank are assumed. Rf phase errors of zero for each cell and 4% for each tank are assumed. The number of particles is 10000.

since the phase width for no-beam loss acceleration is nearly five degrees. In addition, there would be a small beam loss if there were realistic field errors, as shown in Fig. 31. Therefore, a transition energy of 150 MeV is desirable.

2) An FMF of four (1296 MHz) is dangerous from the viewpoint of beam losses.

It should be stressed that the beam-loss problem is most crucial for a high-intensity proton linac. However, the beam quality is also important for a role of injector into the following ring. Therefore, our issue is how to obtain a good beam without any beam loss.

### 3.8.2 Emittance growth

The rf defocusing force is important, since it is related to the transverse emittance growth in a high-accelerating field linac. The amount of nonlinear rf force becomes large when the bunch length becomes large in terms of the phase spread. Thus, a large frequency multiplication factor is not good from this point. Figure 32 shows the transverse rms emittance growth ratio as a function of the injection phase into the CCL. Here, the CCL of 147-MeV injection energy at 972 MHz shows superior properties. The final emittances are listed in Table 13. The final emittances at an energy of 200 MeV are also listed in Table 14. Here, the results for the other configuration, such as DTL+SDTL, is also shown. Figure 33 shows the transverse rms emittance growth ratio when some realistic field errors are assumed. It can be said that there are only small effects on the transverse emittance growth due to the rf field errors.

The longitudinal emittance growth ratio are shown in Figs. 34 and 35. Generally speaking, the longitudinal emittances increase as the rf field errors increase. It should be noted that when the number of lost particles is large, the emittance-growth ratio does not truly reflect the beam properties.

Two conclusions are obtained:

- 1) CCL for a 147-MeV injection energy at 972 MHz shows the most superior beam qualities,
- 2) DTL followed by SDTL shows the most superior beam qualities up to 200 MeV.

### 3.8.3 Injection beam into the DTL

The parameters of the JHP 3-MeV, 324-MHz RFQ have not yet been settled and reported. Thus, a preliminary calculation was performed using the code PARMTEQ to find appropriate parameters of the injection beam into the DTL. The results are summarized in Table 15. Transverse emittances of  $0.8 \pi \text{mm-mrad}$  (90%) and  $1.5 \pi \text{mm-mrad}$  (100%) were used for an injection beam of 30 mA into the RFQ. There are some emittance growths in the RFQ. A drift space between the RFQ and the DTL is necessary in order to achieve both matching and chopping of the beam. Thus, the beam quality at the DTL injection point may be worse than those obtained by calculation. Therefore, the injection emittances into the DTL used in the simulation were

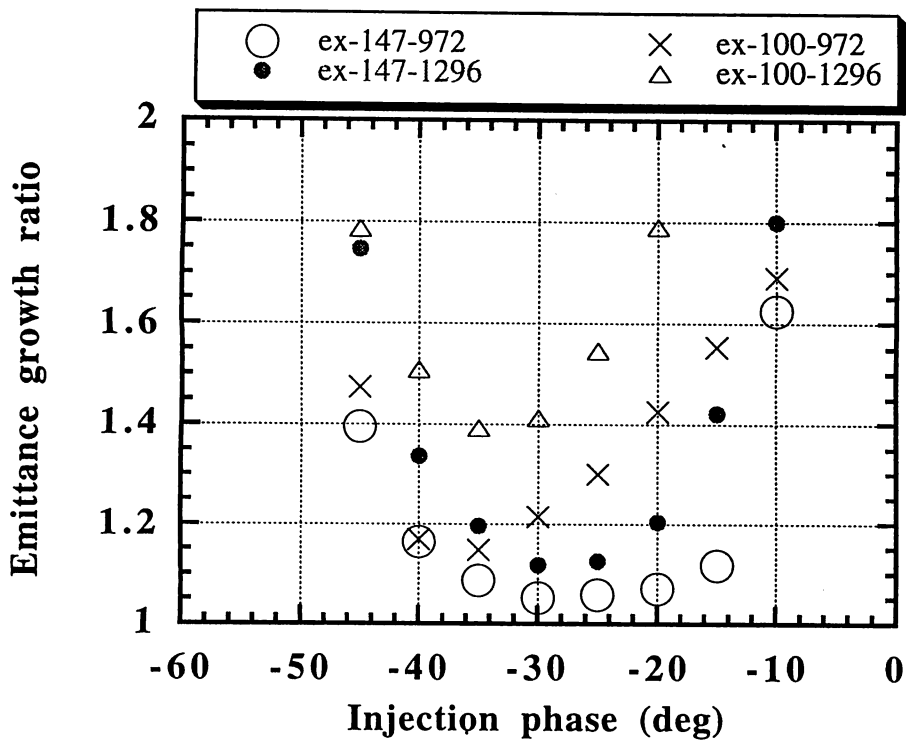


Fig. 32 Rms transverse emittance growth ratio through the CCL as a function of the injection phase for four configurations of the linac. No field errors are assumed. The number of particles is 10000. The indication of 'ex-147-972' means an injection energy of 147 MeV and a frequency of 972 MHz.

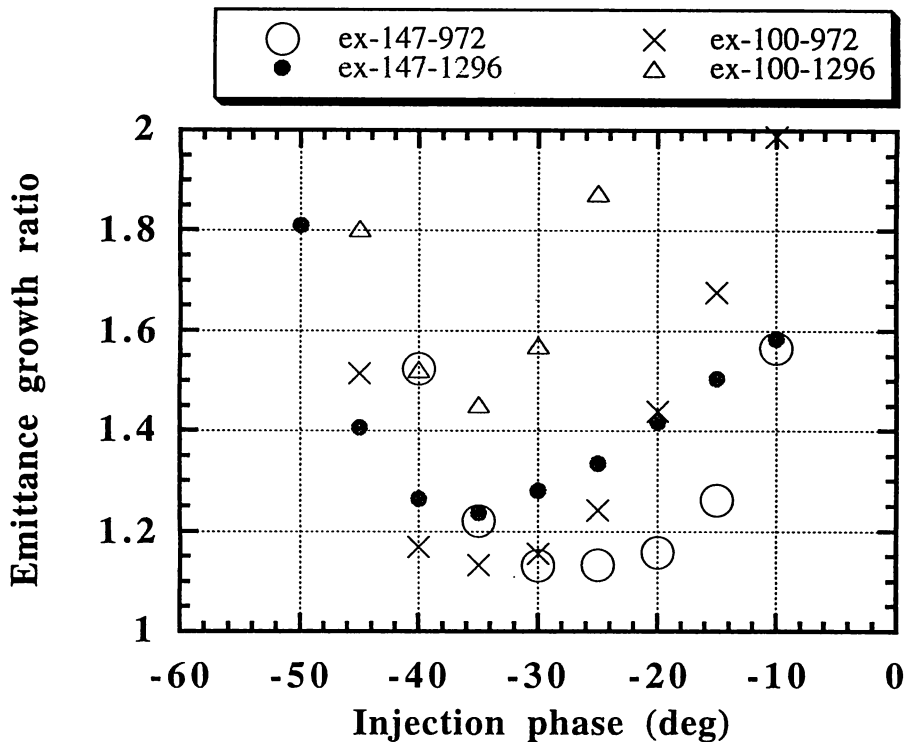


Fig. 33 Emittance (x-x' rms) growth ratio through the CCL as a function of the injection phase for four configurations of the linac. Rf amplitude errors of 1% for each cell and 3% for each tank are assumed. Rf phase errors of zero for each cell and 4% for each tank are assumed. The number of particles is 10000.

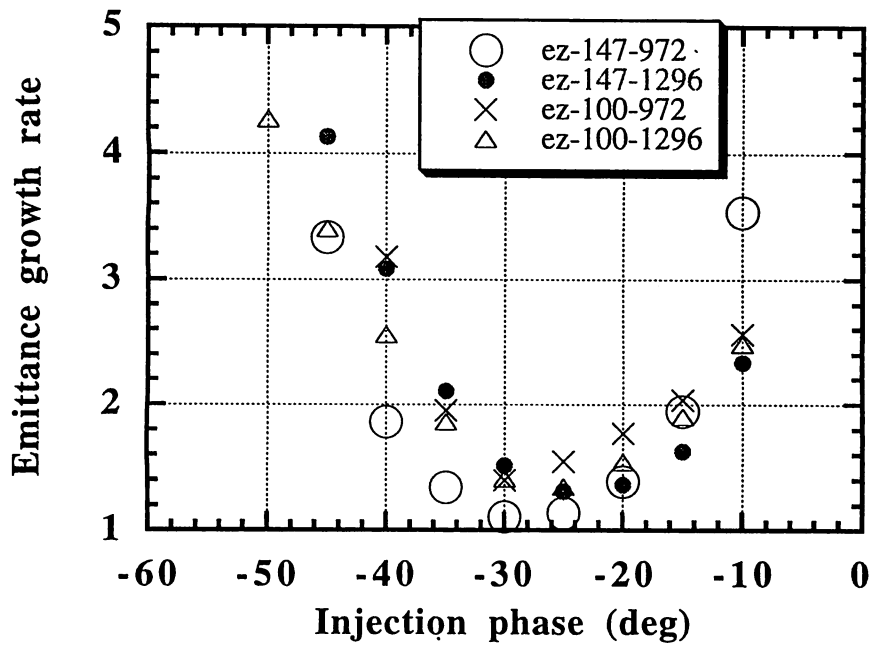


Fig. 34 Rms longitudinal emittance growth ratio through the CCL as a function of the injection phase for four configurations of the linac. No field errors are assumed. The number of particles is 10000.

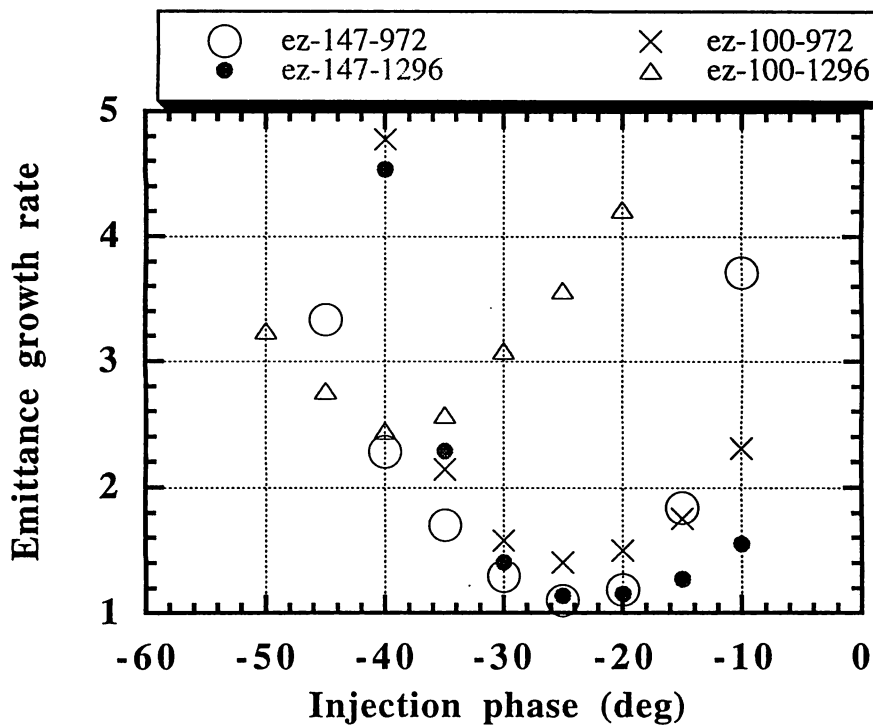


Fig. 35 Rms longitudinal emittance growth ratio through the CCL as a function of the injection phase for four configurations of the linac. Rf amplitude errors of 1% for each cell and 3% for each tank are assumed. Rf phase errors of zero for each cell and 4% for each tank are assumed. The number of particles is 10000.

**Table 13 Final rms emittances for four configurations at the exit of the linac (400 MeV).**

CCL configuration	x	y	z	
	$\pi$ mm-mrad		$\pi$ MeV-deg	
147 MeV - 972 MHz	0.539	0.534	0.468	no beam loss
147 MeV - 1296 MHz	0.572	0.628	0.641	0.18% beam loss
100 MeV - 972 MHz	0.675	0.585	0.600	no beam loss
100 MeV - 1296 MHz	0.733	1.05	0.545	0.12% beam loss

\* z-z' emittances are normalized to those at 324 MHz for comparison.

**Table 14 Final rms emittances for four configurations at the exit of the linac (200 MeV).**

CCL configuration	x	y	z
	$\pi$ mm-mrad		$\pi$ MeV-deg
147 MeV - 972 MHz	0.509	0.523	0.48
147 MeV - 1296 MHz	0.570	0.535	0.51
100 MeV - 972 MHz	0.602	0.843	0.43
100 MeV - 1296 MHz	0.708	1.06	0.48
DTL 51 MeV +SDTL	0.433	0.443	0.364
Injection beam at 3 MeV	0.373	0.379	0.268

\* z-z' emittances are normalized to those at 324 MHz for comparison.

**Table 15 Beam parameters used for the simulations in the low-energy region.**

Results of the preliminary simulation of 3-MeV, 324 MHz RFQ.

Normalized emittances	x			y		
	rms	90%	100%	rms	90%	100%
	$\pi$ mm-mrad			$\pi$ mm-mrad		
Injection into RFQ	0.193	0.822	1.49	0.196	0.831	1.47
Output from RFQ	0.282	1.29	3.04	0.270	1.23	3.34
$\Delta\phi$ (full width)	48.4 degrees					
$\Delta w$ (full width)	116 keV					
Injection beam into the DTL (10000 particles for LINSAC simulation)						
DTL injection beam	0.373	1.59	2.88	0.379	1.61	2.85
$\Delta\phi$ (full width)	50.5 degrees					
$\Delta w$ (full width)	155 keV					

larger than those of the RFQ output beam.

In connection with this point, the CCL simulations using 3200 particles with different emittances generated by the code PARMTEQ show nearly similar results to those using 10000 particles (discussed in previous sections). Figure 36 shows the transmission ratio through the CCL linac. These simulations (shown in Fig. 36) were performed one year before. At that time, the limitation of the supercomputer limited the particle number to 3200. However, the results agree with those with the 10000-particle simulations, although some details are different. Table 16 gives the injection beam parameters. Here, the full energy width of 120 keV is the calculated result through the RFQ. The injection beam parameters are discussed in section 3.7.1 in connection with the matched and equipartitioned condition.

### 3.8.4 Properties of the code LINSAC

The code LINSAC (ref. 9) takes into account the particle-particle interaction for the space-charge calculation (P-P method). Although it gives the correct results for macroscopic properties, some overestimation may be included in the results, mainly in the so-called halo-part of the bunch. This point will be published elsewhere. However, a large collision due to a calculation error can be easily distinguished as follows. Figure 37 shows the emittance growth ratio along the linac. The calculation was performed using 76800 particles. Therefore, a 99.9% emittance can be defined with satisfied accuracy. There is no abrupt change in the emittance-growth ratio. The simulation from 3 to 200 MeV shows an emittance-growth ratio of around 20% for rms and 90% emittances. Figure 38 shows an example for a 10000-particle simulation. In this case, an abrupt change in the emittance-growth ratio can be seen during acceleration, indicating that there was a large collision due to a calculation error. These effects are also observed in the rms emittances, since the rms emittance reflects the effects of all particles. However, these collisional particles can be eliminated by observing the forces between pairs of particles.

The other important point is related to halo-particle formation. It is normally believed that the calculated results become more reliable if the number of macro-particles becomes close to the real number of particles. In connection with this point, the emittance-growth ratio as a function of the number of macro-particles is summarized in Table 17. As for collision effects, there are two ways to verify the code. One is to reduce the emittance of the beam, holding the density constant, in order to use the number of macro-particles, which is equal to the number of particles in a real bunch. The other is to increase the number of macro-particles so as to decrease the macro-charge. By using the first method, the code LINSAC shows accurate results which obey the Rutherford-scattering law. By using the second method, figure 39 shows the radial distribution of the output beam at 147 MeV for two simulations with 10000 and 76800 macro-particles. The two distributions have a similar shape, except for very small differences in the tail part. This kind of calculation is limited by the allowable limit of the calculation time. The output profiles at an energy of 200 MeV are shown in Figs. 40 and 41. A few particles far from the halo part in both figures are due to large collisions, which can be eliminated by monitoring the collisional

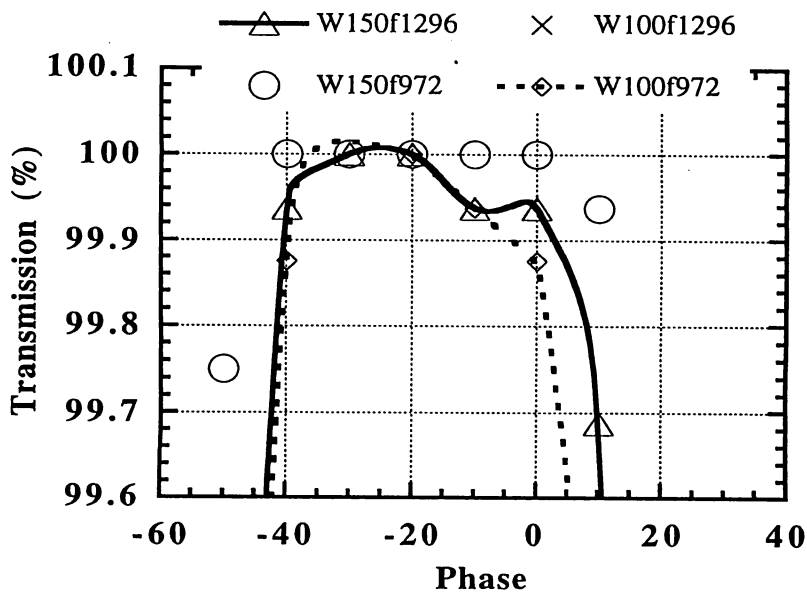
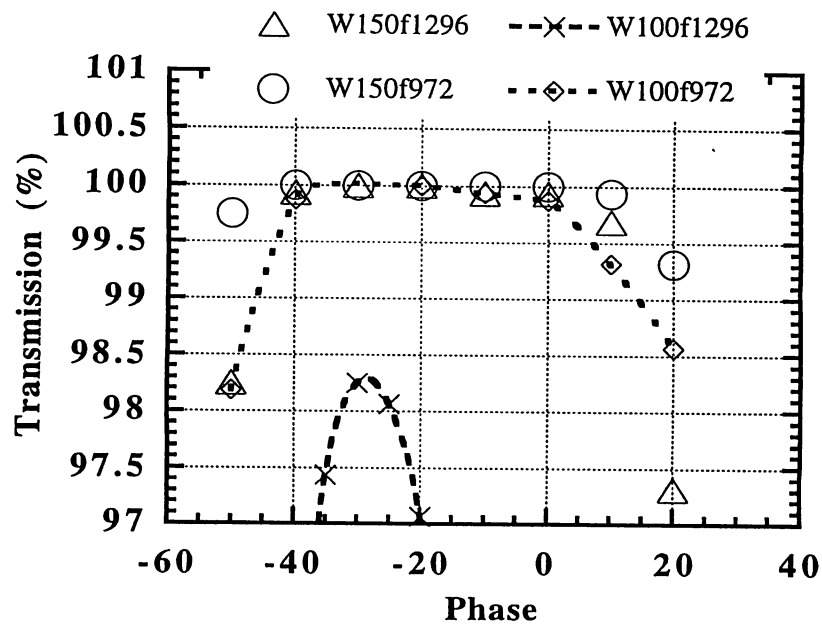


Fig. 36 Transmission ratio through the CCL as a function of the injection phase into the CCL. The number of particles is 3200. The notation 'w150f1296' means an injection energy of 100 MeV and a frequency of 1296 MHz. Both figures show the same results. The ordinate in the lower figure is enlarged.

Table 16 Beam parameters for 3200 injection particles used for the simulations given in Fig.27.

	x			y		
	rms	90%	100%	rms	90%	100%
	$\pi$ mm-mrad:			$\pi$ mm-mrad:		
DTL injection beam	0.314	1.41	3.32	0.30	1.39	3.15
$\Delta\phi$ (full width)	36.1degrees					
$\Delta w$ (full width)	120 keV					

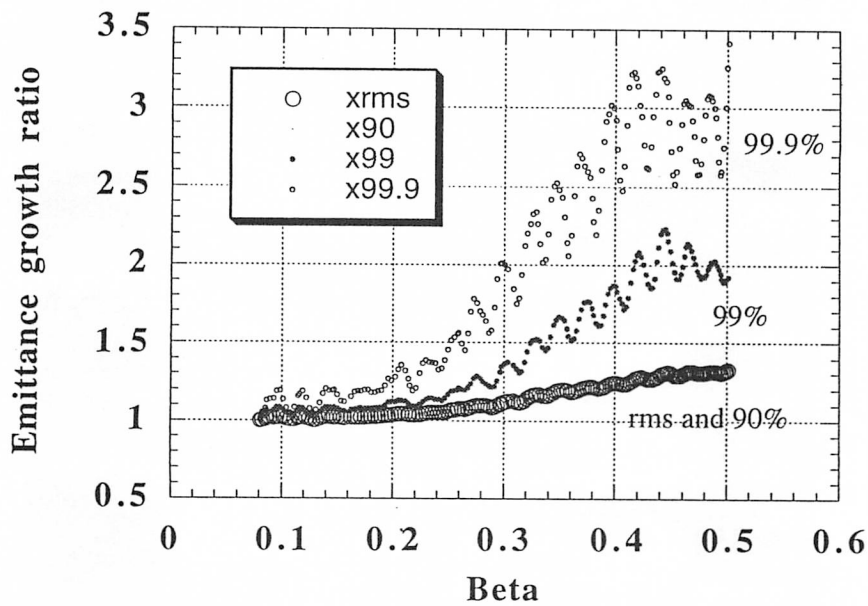


Fig. 37 Relative emittance growth during acceleration in the DTL, calculated with the LINSAC code. The number of particles used was 76800.

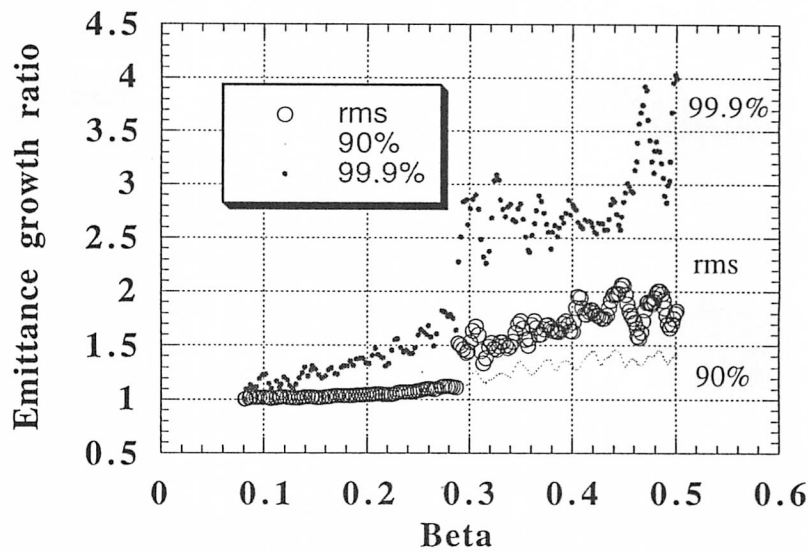


Fig. 38 Relative emittance growth during acceleration in the DTL, calculated with the LINSAC code. The number of particles used was 10000.

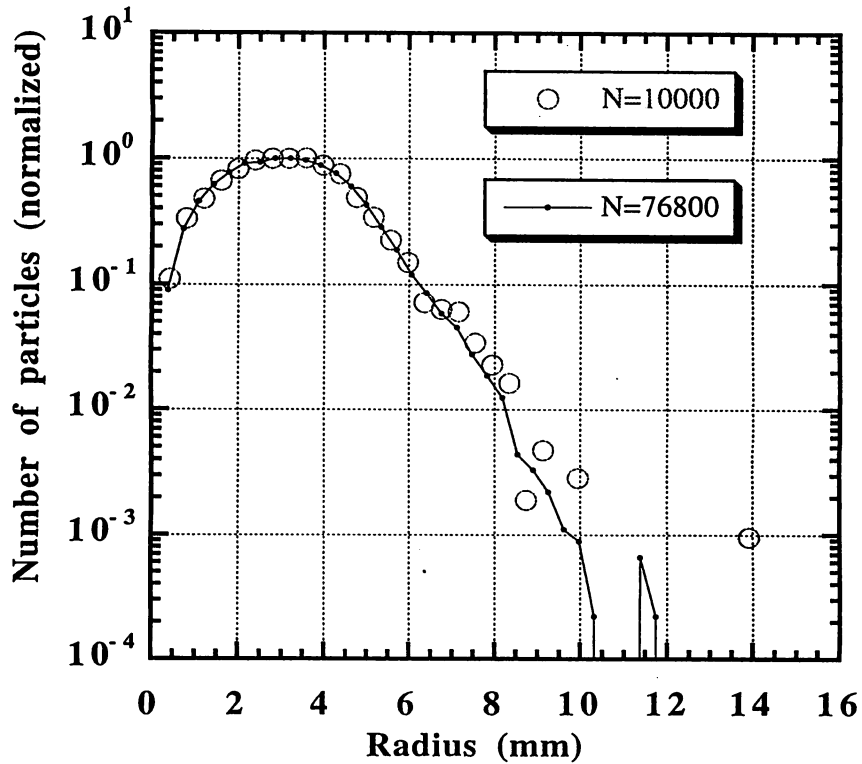


Fig. 39 Radial distribution of the output beam at 147 MeV for two simulations for 10000 and 76800 particles using the code LINSAC.

Table 17 Emittance-growth ratio in the LINSAC simulation. The acceleration was performed from 3 to 147 MeV.

Number of particles	x		y		z	
	rms	90%	rms	90%	rms	90%
10000	1.82	1.40	1.55	1.36	1.7	1.57
19968	1.36	1.35	1.34	1.34	1.56	1.54
76800	1.32	1.32	1.34	1.34	1.57	1.55

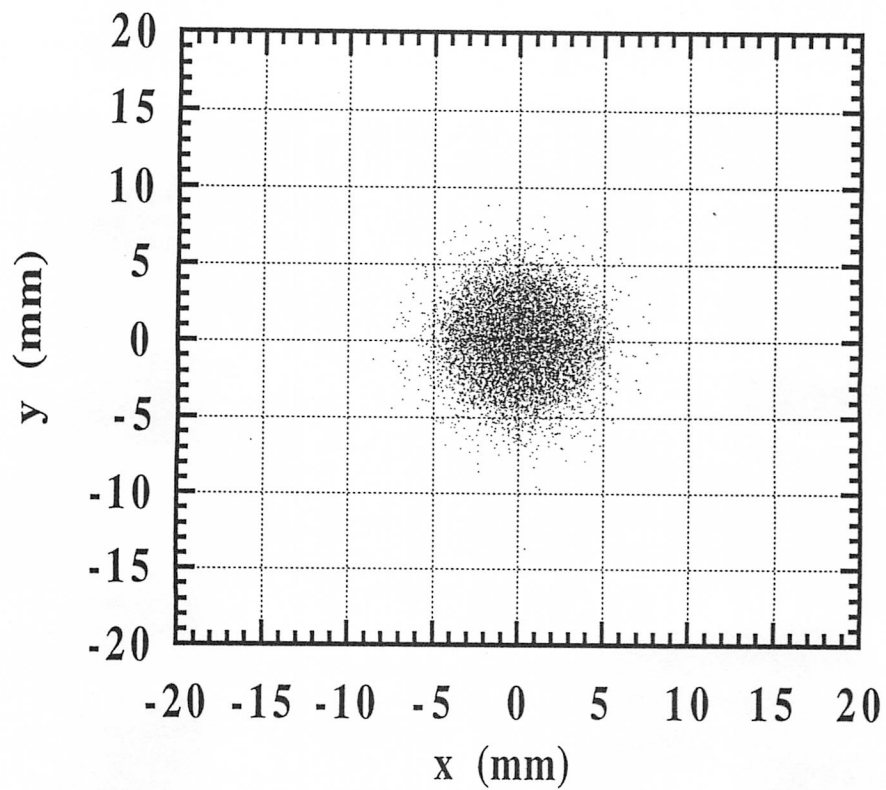


Fig. 40 Profile of the 200-MeV output beam calculated with the code LINSAC. The number of macro particles is 10000.

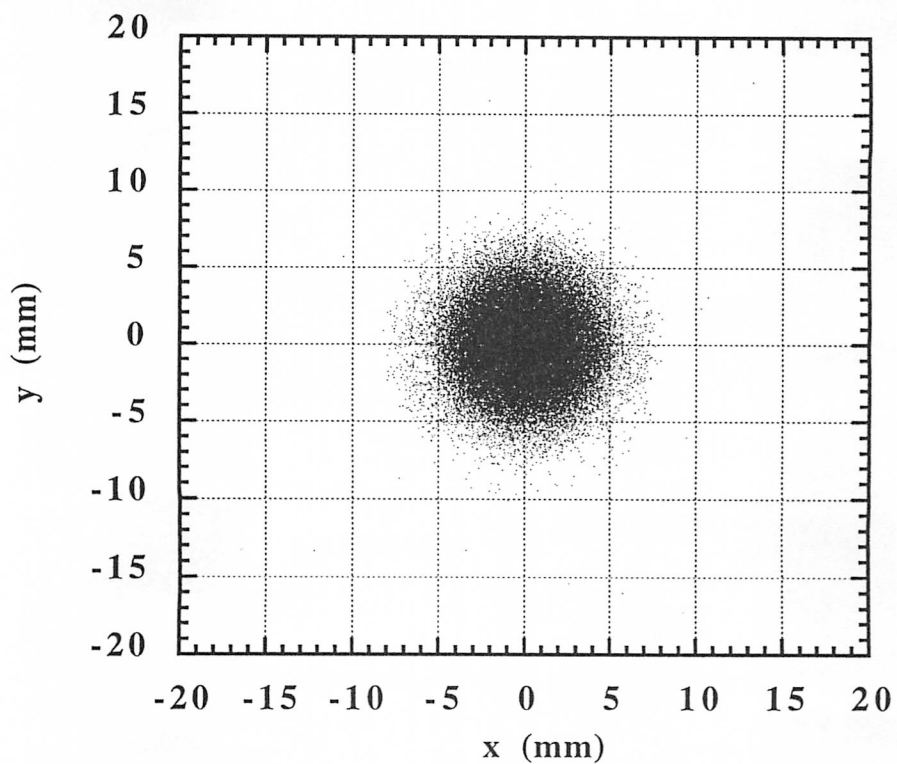


Fig. 41 Profile of the 200-MeV output beam calculated with the code LINSAC. The number of macro particles is 76800.

forces between all pairs of particles if necessary.

### 3.9 CCL of 648 MHz

There is possibility for adopting a 648-MHz CCL-type structure with a rather lower injection energy below 100 MeV. Thus, three kinds of beam simulations were performed using the code PROEND. The injection particles into the CCL at an energy of 70 MeV was made by acceleration through the DTL using the code LINSAC.

#### 1) CCL-648-A

First, a stable phase angle of -30 degrees and a tank length of about 1.5 m (number of unit cells in a tank is 18) were selected. This geometry gives an rms transverse acceptance of  $5\pi$  mm-mrad. There are always some beam losses of more than 0.14% when the particles are injected with only transverse matching. They are improved up to 0.01% with the injection of both transverse and longitudinal matching. If the beam is injected without an additional phase spread due to the double frequency and the drift length between the DTL and the CCL, there is no beam loss up to 400 MeV. Either the additional phase spread due to the double frequency or due to the drift length of 2 m causes beam losses in this case.

#### 2) CCL-648-B

Next, a tank length of 1.36 m (number of cells is 16) was tried. This improved both the transverse and longitudinal acceptances compared with those in the CCL-648-A. The injection beam into the CCL was matched in the transverse motion. There is no beam loss in injection with a stable phase angle. However, if the injection phase changes by five degrees from the stable phase angle, there are beam losses of 0.03%. A simulation with both transverse and longitudinal matching injection does not increase the transmission ratio in this case. The phase acceptance for completely stable acceleration is below five degrees.

#### 3) CCL-648-C

There is a method for increasing the phase acceptance by introducing a larger (absolute value) stable phase angle. First, similar simulations were performed with a varied stable phase angle from -40 to -30 degrees during eight initial unit tanks. However, a phase acceptance for completely stable acceleration of more than five degrees could not be achieved. Then, a varied phase stable angle of from -50 to -30 degrees during the initial 16 unit tanks was tried. In this case, a phase acceptance of more than five degrees could be obtained for the transverse-matching simulation. The transmission ratio is plotted in Fig. 42. In this simulation, nearly the same results for both transmission and emittance growth as those obtained with a frequency of 972 MHz and an injection energy of 147 MeV were achieved. These results (summarized in Table 18) can be obtained at the cost of acceleration efficiency and the total accelerator length. The results for an output energy of 200 MeV are also given in Table 19. Here, the effects of our

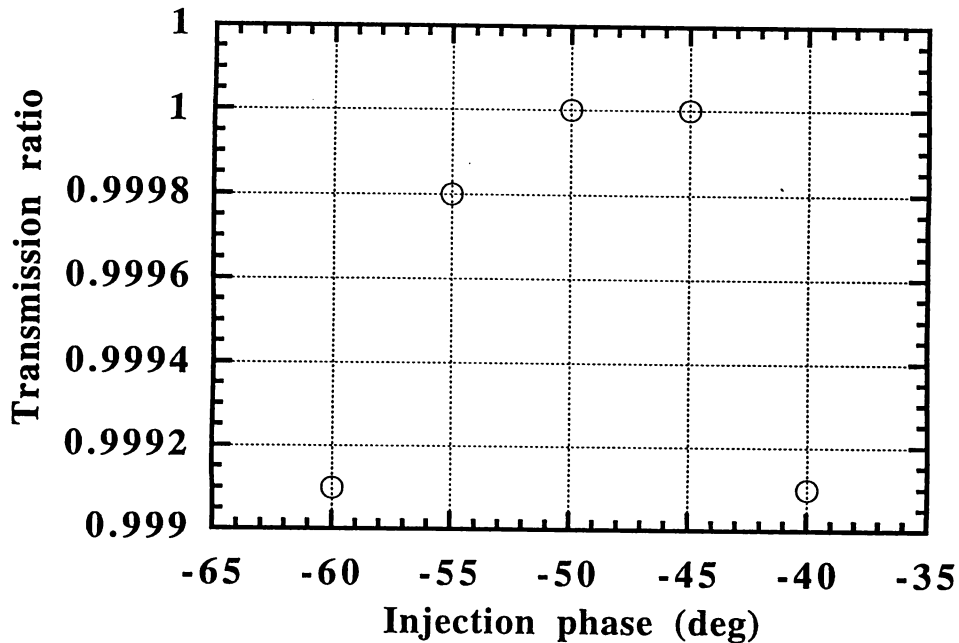


Fig. 42 Transmission ratio through the CCL-648-C system. The injection energy into the CCL structure at a frequency of 648 MHz is 70 MeV

design strategy to avoid a nonlinear field and to achieve maximum accelerating efficiency can be seen more clearly by a comparison of the transverse emittances and rf power consumption given in Table 19. It is commonly pointed out that any types of perturbations in connection with nonlinearity cause disastrous effects in a high-intensity linac. In conclusion, although a transition at around 70 MeV is possible, it is possible at the cost of an acceleration efficiency of 28% (an additional power of 12 MW for the 400-MeV system). After that, the phase acceptance for the stable acceleration without beam losses is not very wide.

Finally, the accelerator configurations mentioned in section 3.6.6 were re-examined by using a varied stable phase angle if necessary. The results are listed in Table 20. The following items are pointed out:

- 1) The difference in length and rf power between No.8 and No.9 is not very large.
- 2) The acceleration efficiency of ACS-648 MHz (No.6 and 13), which has no cooling channel around the nose-corn part, is not very high among others, in spite of the cooling-less critically operating structure.
- 3) The decrease in the accelerating efficiency due to the effects of tuning of the stable phase angle is clearly observed by comparing those with lower transition energies and those with higher transition energies into the CCL structure.
- 4) Those systems using the SDTL structure show a superior acceleration efficiency.

### 3.10 CCL of 972 MHz with an injection energy of 100 MeV

**Table 18 Comparison of the final emittances at 400 MeV among the CCL simulations of 648 MHz.**

	x	y	z	Total length	Total power
	$\pi$ mm-mrad			m	MW
CCL-648-A(1)	0.458	0.508	0.333	207.8	60.3
CCL-648-B(2)	0.519	0.489	0.423	200.8	63.6
CCL-648-C(3)	0.524	0.464	0.394	206.9	65.2
DTL+SDTL+ACS	0.516	0.531	0.58	201.6	53.7

remark (1) There are always beam losses of more than 0.14% when only transverse matching is applied. A stable phase angle of -30 degrees is maintained throughout the acceleration.

remark (2) There is no beam loss in stable phase injection. There are beam losses of more than 0.03% when the injection phase shifts 5 degrees from the stable phase angle. A stable phase angle of -30 degrees was chosen.

remark (3) The stable phase angle varies from -50 to -30 degrees during initial 16 tanks. A phase acceptance of more than five degrees is achieved.

**Table 19 Comparison between the optimised SDTL system and the CCL of 648 MHz at the output energy of 200 MeV.**

	Output emittances (rms/90%, $\pi$ mm-mrad, MeV-deg)			Total length	rf power
	x	y	z	m	MW
DTL + SDTL	0.433/1.89	0.443/1.91	0.364/1.44	120.9	27.3
DTL + CCL-648-C	0.475/2.11	0.472/2.07	0.402/1.64	118.3	31.3

It has already been shown in section 3.8 that a CCL structure of 972 MHz with a 100-MeV injection energy shows some beam losses if a stable phase angle of -30 degrees is chosen. In order to achieve stable acceleration without beam losses, a lower stable phase angle is chosen and varied during acceleration, as mentioned in the previous section. First, the stable phase angle was varied from -40 to -30 degrees during the initial 16 tanks. An acceleration without beam losses was achieved only around an injection phase of -35 degrees. Therefore, the phase acceptance for stable operation is so narrow that more phase acceptance is desirable. Here, only transverse matching was considered. Next, the stable phase angle was varied from -50 to -30 degrees (named system-D). In this case, a phase acceptance of more than five degrees could be obtained. Figure 43 shows the transmission ratio. The main parameters are summarized in Table 21. Our conclusions are as follows:

**Table 20 Summary of the calculated total length and rf power for important candidates of a linac complex. Here, a stable phase varies along the linac in order to accept all of the injected particles from the DTL.**

System	Pc		Pb		Ptot		Lrf m	Ltot mA
	MW		30	60	30	60		
<b>200 MeV</b>								
1. DTL-50MeV+SDTL	17.52	21.33	5.98	11.96	27.31	33.29	92.91	120.87
2. DTL-50MeV+SDTL-148MeV+ACS972	16.63	20.26	5.97	11.94	26.23	32.20	85.30	110.71
3. DTL-70MeV+ACS-648MHz	22.77	27.78	5.99	11.97	33.77	39.75	87.85	118.30
4. DTL-100MeV+ACS-648MHz	21.07	25.28	6.00	12.00	31.28	37.28	73.84	110.68
5. DTL-100MeV+ACS-972MHz	19.69	24.34	5.91	11.82	30.25	36.16	90.11	112.32
6. DTL-100MeV+ACS-648MHz-no-water	18.79	22.55	6.08	12.16	28.63	34.71	76.87	109.74
7. ALL-DTL	17.94	23.32	5.92	11.84	29.24	35.16	126.80	138.73
<b>400 MeV</b>								
8. DTL-50MeV+SDTL-148MeV+ACS972	34.48	41.69	11.99	23.98	53.67	65.66	149.28	201.64
9. DTL-50MeV+SDTL200MeV+ACS972	35.28	42.64	11.97	23.94	54.61	66.58	156.51	216.27
10. DTL-70MeV+ACS-648MHz	43.99	53.25	11.97	23.94	65.22	77.19	144.81	206.89
11. DTL-100MeV+ACS-648MHz	42.14	50.57	11.94	23.89	62.51	74.46	130.41	201.57
12. DTL-100MeV+ACS-972MHz	39.92	48.62	11.90	23.79	60.50	72.41	144.45	196.08
13. DTL-100MeV+ACS-648MHz-no-water	35.85	43.02	12.03	24.06	55.04	67.07	137.78	198.20

\* Pc.mod includes the rf multiplying factor.

- 1) The rf power of the SDTL system (up to 400 MeV) is smaller than that of system-D by about 7 MW .
- 2) The final transverse emittances for system-D is larger than those for the SDTL system by 30 - 40 % at 200 MeV, and 14 - 18 % at 400 MeV.
- 3) The final longitudinal emittances for system-D is larger than those for the SDTL system by 32% at 200 MeV, and -4% at 400 MeV.
- 4) A stable region of injection phase is about five degrees for system-D, implying the requirement of difficult tuning of the accelerating parameters and expected beam losses during operation due to other error effects.

A linac complex (system-D), consisting of a 100-MeV DTL and a 972-MHz CCL, is dismissed due to the reasons mentioned above.

Recently, two kinds of beam measurements, valuable and helpful for our design work, have been reported. The first is a measurement of the beam parameters of the CERN proton linac at an energy of 50 MeV using a three-dimensional bunch shape monitor (ref. 10). It has been reported that the longitudinal bunch consists of a core part, which can be explained by the existing theory and simulation, and a rather large tail part, which can not be easily explained. The second is a beam-loss measurement at the Fermilab 400-MeV linac, which was extended

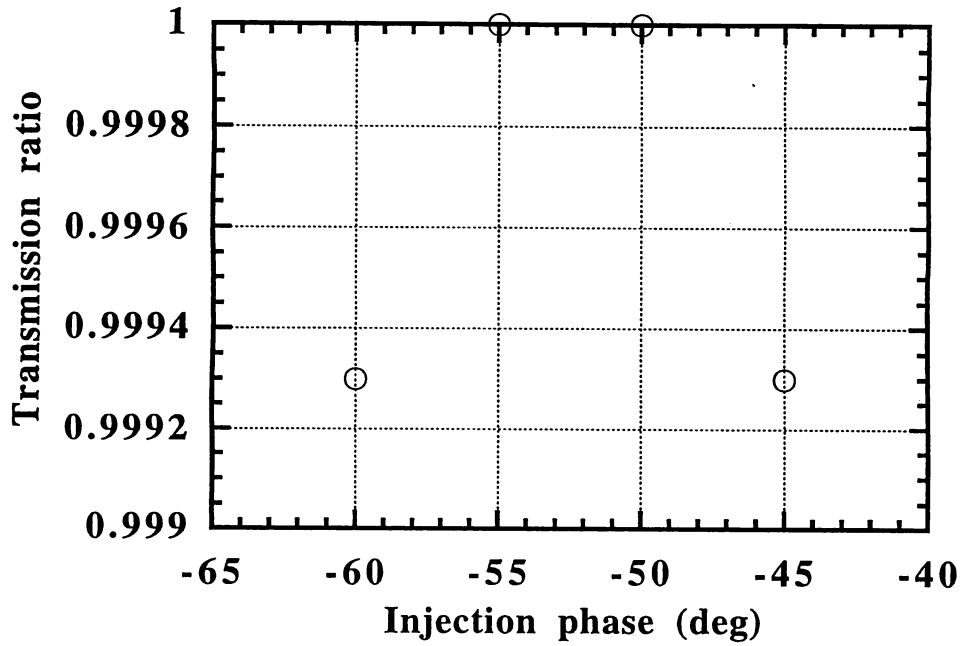


Fig. 43 Transmission ratio versus the injection phase angle for the CCL 972 MHz system with an injection energy of 100 MeV. The stable phase angle varies from -50 to 30 degrees during the initial 16 unit tanks.

Table 21 Comparison between the optimised SDTL system and CCL of 972 MHz with a 100-Mev injection energy.

	Output emittances (rms/90%, $\pi$ mm-mrad, MeV-deg)			Total length m	rf power MW
	x	y	z		
400 MeV					
DTL + SDTL+ACS	0.516/2.23	0.531/2.26	0.577/2.24	201.6	53.7
DTL + CCL-972	0.608/2.70	0.607/2.68	0.553/2.39	196.1	60.5
200 MeV					
DTL + SDTL	0.433/1.89	0.443/1.91	0.364/1.44	120.9	27.3
DTL + CCL-972	0.562/2.46	0.614/2.82	0.480/1.99	112.3	30.3

using the CCL structure of four-times the DTL-frequency above 116 MeV (ref. 11). They observed beam losses of less than 2%. The magnitude of the beam loss is nearly the same as our simulation (Fig. 30 in section 3.8.1). Therefore, it can be said the two reports indirectly support our simulation results.

## 4. RF source

The rf power source is one of the key issues of a linac. There are two types of rf systems: one uses vacuum tubes, such as triodes or tetrodes, and the other uses klystrons. We have decided to adopt klystrons for all frequencies. One of the key issues of the rf system is setting the maximum available peak power from the klystrons. This has effects upon not only the rf systems but also the configuration of the accelerating structure. Generally speaking, a design with a larger peak power reduces the number of klystrons and related rf equipment, resulting in a reduction of the rf cost. However, it is known by experience that the number of troubles related to a high-power rf source tends to increase as the handling peak power approaches the allowable maximum power. It is also widely known that the available peak power from the klystron depends upon both the rf pulse length and the repetition rate. Therefore, a compromise among many related items is required in order to determine the peak power of the klystrons. It is concluded in section 3.7 that a klystron of 2.5 - 3 MW peak power is desirable.

### 4.1 Power dividing method for SDTL unit tanks

Figure 44 shows the rf driving power, beam power and total power for the unit tanks of the SDTL structures. Because of adopting a rather high accelerating field, the total power required for a unit tank varies from 0.48 to 0.89 MW. Assuming 3-MW klystrons, there are two ways to supply rf power into the unit tank. One is to use bridge-couplers between adjacent unit tanks. The other is to use a power divider to feed each unit tank. It is known that both the DTL and SDTL structures are driven by  $2\pi$ -mode operation, in which the group velocity is zero. Thus, some devices for stabilizing the structure are required under heavy beam-loading operation. For the DTL structure, additional post couplers can stabilize the field. For SDTL structures combined by bridge couplers, additional post couplers are necessary to stabilize the field. On the contrary, for SDTL structures driven through power dividers, some devices for stabilizing the field are not necessary, since an rf coupler drives only several numbers of unit cells. In addition, the size of the waveguide, corresponding to a frequency of 324 MHz, seems to be too large to install a waveguide-type bridge coupler between two SDTL tanks. In conclusion, it seems better to use a power divider to feed rf power into a few numbers of unit tanks from a klystron.

### 4.2 Field errors due to a change in the beam current

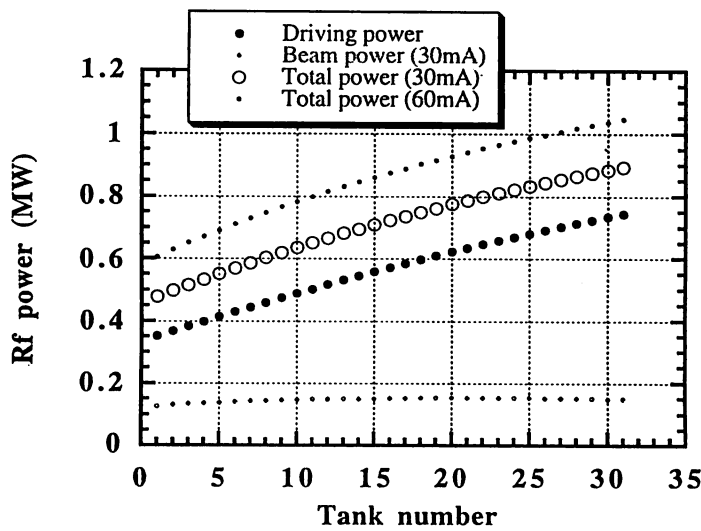


Fig. 44 Required rf power for the SDTL tanks. Beam currents of 30 and 60 mA are assumed.

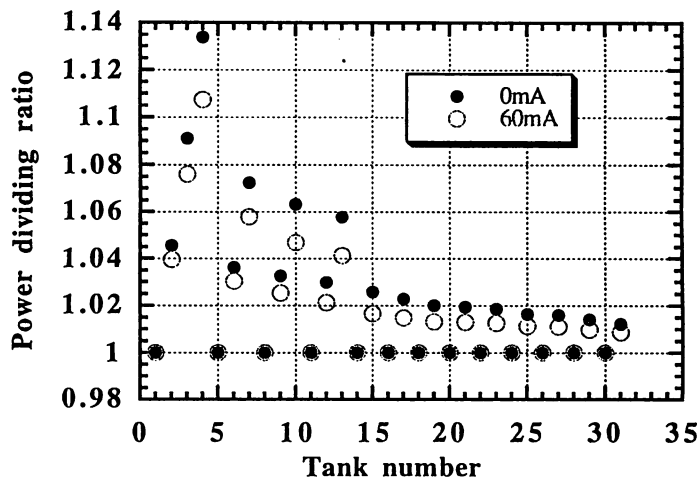


Fig. 45 Relative required power ratio among SDTL tanks driven by klystrons of the same amount of an rf output. In the system, there are one four-combined tanks, three three-combined tanks and nine two-combined tanks.

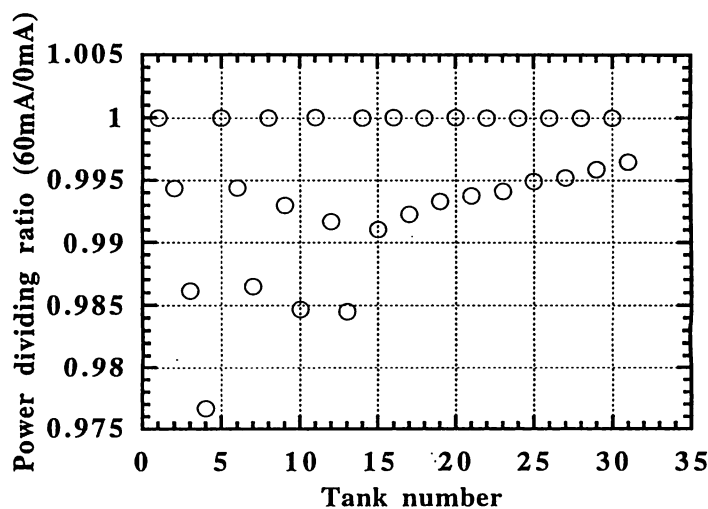


Fig. 46 Ratio between the power dividing ratio with zero current and that with 60 mA

Assuming a 3-MW peak power klystron, the first klystron supplies rf power to the first four successive SDDL tanks. The next three klystrons supply rf power to three successive SDDL tanks, and the other klystrons supply two successive SDDL tanks. Figure 45 shows the relative required power ratio for the tanks driven by klystrons. Here, the required rf power is normalized by that for the first tank in each rf dividing set. Since the shunt impedances vary with the energies, the required rf power for each tank driven by a klystron also changes by 14% within the first rf dividing set, for example. The required rf power also depends upon the beam loading. Thus, once the rf power is correctly divided according to the required value with zero current, the errors increase as the beam loading increases. Figure 46 shows the ratio between the power dividing ratio with zero current and that with 60 mA. In this case, a 2.5%-error in rf power is inevitable among four tanks driven by the first klystrons. In order to reduce this, a smaller number of power dividing is desirable. Thus, our final design assumes 2.5-MW peak-power klystrons, driving three and two tanks. Similar phenomena also occur in rf driving systems using bridge couplers as a power-dividing device.

## 5. Beam-transport line between the RFQ and the DTL

### 5.1 General design

In order to match the RFQ beam with the DTL acceptance, a beam-transport line is necessary. In the DTL section, there is strong acceleration, which has effects upon both the transverse and longitudinal motions. It thus seems to be difficult to match the beam as well as acceleration simultaneously, while keeping the relation between two freedoms of motion constant, since there is not many free focusing parameters which can have their effects verified by measurements. Therefore, we perform a matching process and acceleration independently.

Typical parameters for the beam-transport line for a frequency of 432 MHz have already been reported in ref. 12. The design for a frequency of 324 MHz will be performed on the basis of the 432-MHz design, and will be reported elsewhere.

### 5.2 Buncher

A buncher is necessary to match the beam with the DTL longitudinal acceptance. In principle, a two-buncher system is desirable; however, a beam-simulation result shows that a one-buncher system is sufficient. Typical parameters of the buncher cavity has already been reported in ref. 12 at a frequency of 432 MHz.

### 5.3 Chopper

In order to reduce beam losses after injection into the following ring, a fast beam chopper

system is required. We have concluded that the beam-transport line between the RFQ and the DTL is suitable for this purpose. A preliminary design of a new-type rf chopper of 432 MHz has already been reported in ref. 13. Therefore, some modifications are required for a 324-MHz rf chopper.

## 6. Debuncher for output beam

In order to satisfy the requirement for the energy spread of the linac output beam, a debuncher located downstream of the exit of the linac is necessary. We assume a required momentum spread of  $\Delta p/p=0.1\%$ , and thus a 90% half energy spread of 365 keV. The results of a preliminary calculation are shown in Fig. 47. In this case, an ideal acceleration was assumed, resulting in an output-energy spread of 330 keV and a phase spread of 6.1 degrees. Therefore, a debuncher is not necessary. Next, an injection phase error of -10 degrees was assumed in the SDTL acceleration, resulting in an output-energy spread of 698 keV and a phase spread of 14.0 degrees. The results of the debuncher operation are shown in Fig. 48. In this case, a debuncher of 1.5 MV voltage at 30 m downstream from the exit of the linac or 0.8 MV voltage at 40 m downstream is required.

## 7. Lorentz stripping of $H^-$

An electron of the  $H^-$  ion is easily dissociated by a magnetic field, which is equivalent to an electric field of  $E = \beta\gamma cB$  in relativistic kinematics. The lifetime in the rest-frame is given as

$$\tau = \frac{A_1}{E} \exp\left(\frac{A_2}{E}\right),$$

where  $A_1 = 2.47 \times 10^{-6}$  V-s/m and  $A_2 = 4.49 \times 10^9$  V/m (ref. 14). The lifetime in the laboratory frame is given by

$$\tau_f = \gamma\tau,$$

where  $\gamma$  is the Lorentz contraction factor. The ratio of dissociation ( $f$ ) is given by

$$f = \frac{T}{\tau_f},$$

where  $T$  is the transit time factor along the magnet. When a maximum allowable value of  $6.1 \times 10^{-6}$  is assumed in our case, the maximum magnetic fields become

$$200 \text{ MeV: } B_{\max} = 0.88 \text{ T and } dh/dz=0.433,$$

$$400 \text{ MeV: } B_{\max} = 0.6 \text{ T and } dh/dz=0.19,$$

where  $h$  is the deflecting length and  $z$  is the coordinate toward the moving direction. With a safety margin of 20%, the allowable values become as follows:

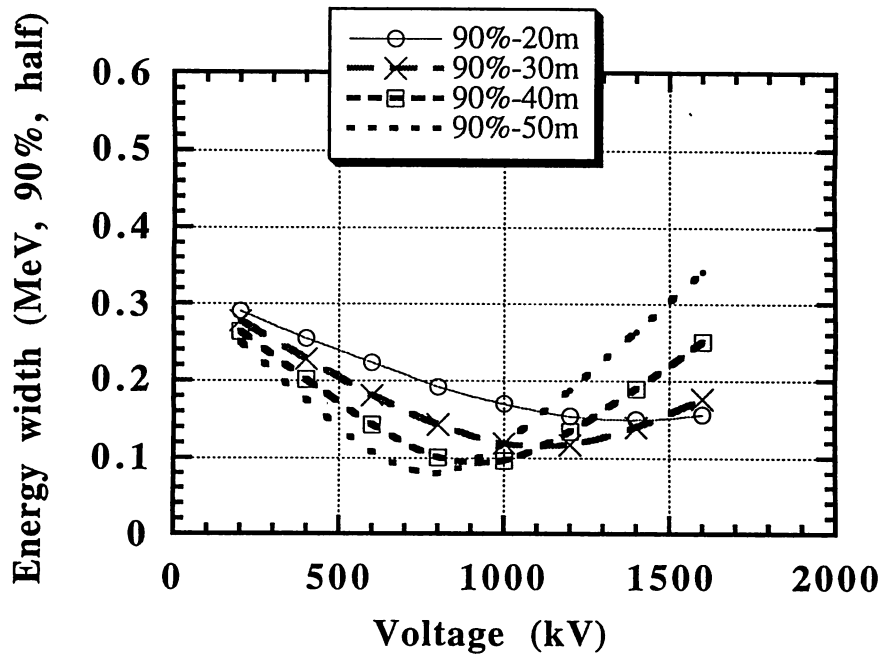


Fig. 47 Energy width of the output beam as a function of the debuncher voltage and the drift spaces between the exit of the linac and the debuncher. An ideal acceleration in the SDTL is assumed.

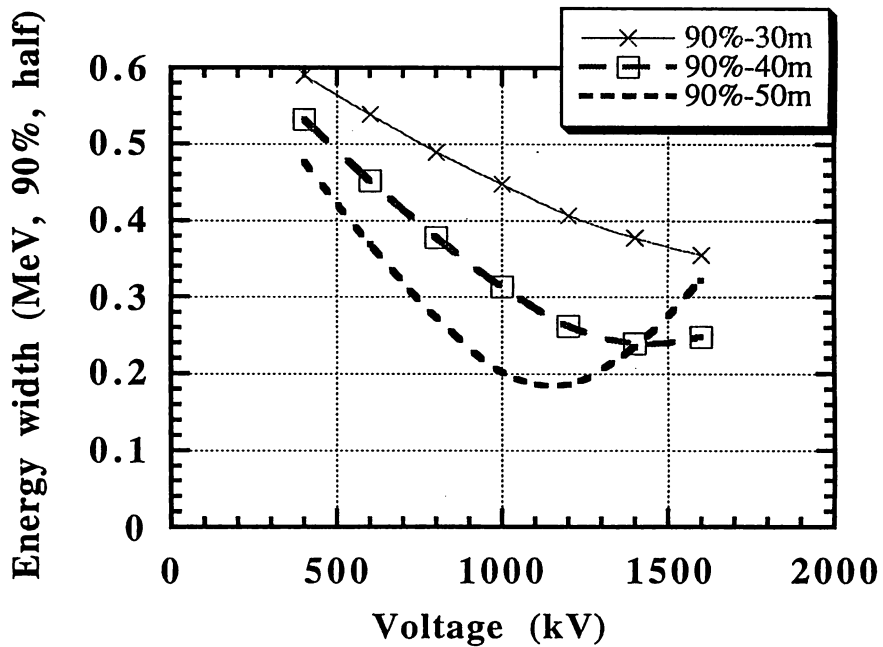


Fig. 48 Energy width of the output beam as a function of the debuncher voltage and the drift spaces between the exit of the linac and the debuncher. An injection phase deviation of 10 degrees into the SDTL is assumed.

200 MeV  $B=0.7$ ,  $f=8.39e-9$ ,  $dh/dz=0.338$ ,  $r=3.07$  m,  
 400 MeV  $B=0.48$ ,  $f=9.22e-9$ ,  $dh/dz=0.152$ ,  $r=6.63$  m,

where  $r$  denotes the bending radius, given by

$$Br = \frac{1}{300}(T^2 + 2TW_0)^{1/2}.$$

Here,  $T$  is the kinetic energy (MeV) and  $W_0$  the rest mass (MeV). The loss fraction by a 1-m long magnet was calculated and is shown in Fig. 49 as a function of the bending radius.

## 8. Upgrade of the output energy

Three desirable upgrade plans up to an output energy of 400 MeV are as follows:

- 1) DTL + SDTL (200 MeV) + ACS (972 MHz),
- 2) DTL + SDTL (200 MeV) + ACS (1296 MHz),

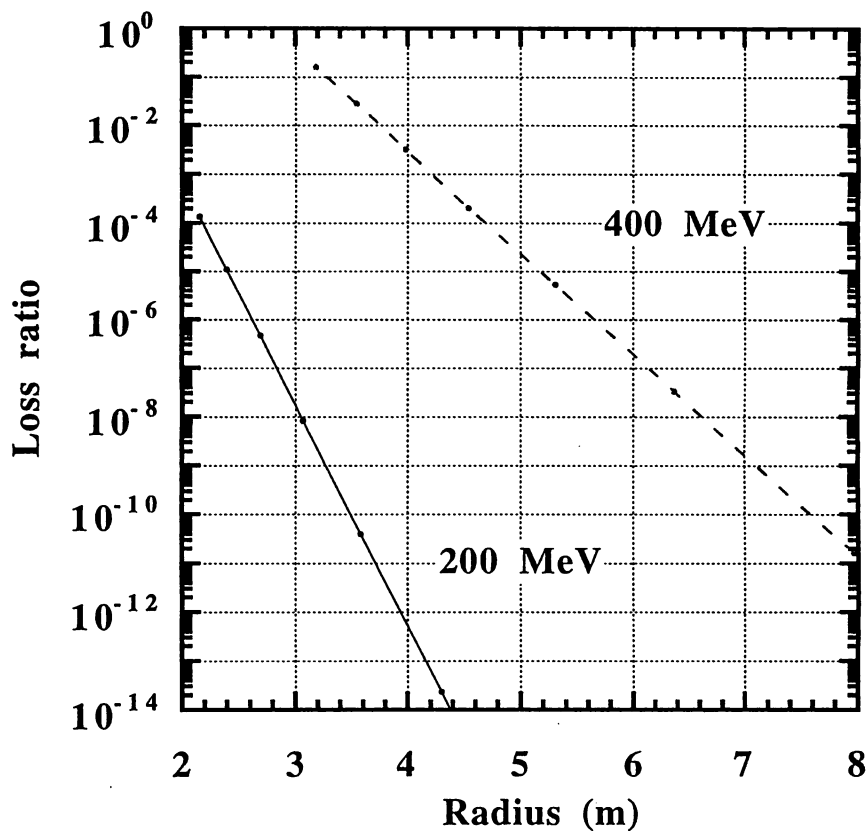


Fig. 49 Loss ratio per unit length by Lorentz stripping for 200 and 400 MeV negative hydrogens.

### 3) DTL + SDDL (150 MeV) + ACS (972 MHz).

The first and second plans add a CCL section to the existing linac. The choice of the operating frequency depends upon the beam quality at the exit of the 200-MeV linac and the results of beam simulation in the CCL part. The third plan removes a part of the existing linac and adds a CCL of 972-MHz. When a transition energy of around 150 MeV is selected, a frequency multiplication factor of three is recommended according to our simulation results. It is desirable and necessary to determine the important parameters by accumulated experience and studies. Fortunately, we will have a chance to study the properties of an output beam of 200 MeV. In addition, as far as a maximum energy of 200 MeV is concerned, the best choice is that there be no frequency transition throughout the linac. Therefore, a final determination of the CCL operating frequency should be put off to the future. Here, two plans ((1) and (3)) are summarized in Tables 22 to 25.

## 9. Summary of the design

A 200-MeV proton linear accelerator for Japanese Hadron Project (JHP) has been designed. It consists of a 3-MeV radio-frequency quadrupole linac (RFQ), a 50-MeV drift tube linac (DTL) and a 200-MeV separated-type drift tube linac (SDDL). A frequency of 324 MHz has been chosen for all of the rf structures. A peak current of 30 mA ( $H^+$  ions) of 400  $\mu$ sec pulse duration will be accelerated at a repetition rate of 25 Hz. A future upgrade plan up to 400 MeV is also presented, in which an annular-coupled structure (ACS) of 972 MHz is used above 150 or 200 MeV. The important features of the design are as follows:

- 1) High performance for beam-loss problem during acceleration can be achieved by separating the transition point in the transverse motion from that of longitudinal motion. The transverse transition at a rather low-energy range decreases the effects of space-charge, while the longitudinal transition at a rather high-energy range decreases the effects of nonlinear problems related to acceleration in the ACS.
- 2) The coupled envelope equations and the equipartitioning theory are used for the focusing design.
- 3) The adoption of the SDDL structure improves both the effective shunt impedance and difficulties in fabricating drift tubes with focusing magnets.
- 4) Simple mechanical structures for accelerators are selected.
- 5) Klystrons are used.
- 6) Acceleration ability for an increase in the peak current up to 60 mA is included.
- 7) Smooth upgrade potentiality up to 400 MeV is considered. The transition energy from SDDL to ACS should be determined by using directly accumulated beam data in the future. There are presently two candidates, 150 and 200 MeV.
- 8) The accurate beam-simulation code on a parallel supercomputer was used for confirming the beam-loss problem during acceleration.

The main parameters are summarized in Table 26. The effective shunt impedances for the three structures are given in Fig. 50.

### Acknowledgments

The author wishes to express his gratitude to Y. Yamazaki and the members of the 1-GeV linac working group for stimulating discussions. He also wishes to give thanks to L. V. Kravchuk and Y. V. Senichev for valuable discussions.

### References

1. A. Schempp et al., "RFQ-, Chopping- and Funneling-studies for the ESS-Injector-Linac," Proc. 1996 International Linac Conf., to be published.
2. A. Ueno and Y. Yamazaki, "Rf Field Measurement of a Four-Vane Type RFQ with PISLs," Proc. 1992 Linear Accelerator Conf., p.713 (1992).
3. A. Ueno et al., "Beam Test of the Pre-Injector and the 3-MeV  $H^-$  RFQ with a New Field Stabilization PISL," Proc. 1996 International Linac Conf., to be published.
4. F. Naito et al., "Rf Characteristics of a High-Power Model of the 432 MHz DTL," Proc. 1994 International Linac Conf., p.137 (1992).
5. T. Kato, "Proposal of a Separated-Type Proton Drift Tube Linac for a Medium-Energy Structure," KEK Report 92-10.
6. T. Kageyama et al., "Development of Annular Coupled Structure," Proc. 1994 International Linac Conf., p. 248 (1994).
7. Y. Namito in Radiation Safety Control Center at KEK, private communication.
8. M. Reiser, "Theory and Design of Charged Particle Beams," Section 5, John Wiley & Sons, 1994.
9. T. Kato, "Beam Simulation Code Using Accurate Gap Field Distributions in a Drift Tube Linac," Proc. 1994 International Linac Conf., p.523 (1994).
10. A. V. Feschenko et al., "Study of Beam Parameters of the CERN Proton Linac Using a Three Dimensional Bunch Shape Monitor," Proc. 1996 International Linac Conf., to be published.
11. L. J. Allen et al., "Operation and Improvements of the Fermilab 400 MeV Linac," Proc. 1996 International Linac Conf., to be published.
12. T. Kato, "Design of Beam-Transport Line between the RFQ and the DTL for the JHP 1-GeV Proton Linac," Proc. 1994 International Linac Conf., p.59 (1994).
13. T. Kato, "New Design of an RF Beam Chopper," Proc. 7th Symposium on Accelerator Science and Technology, p.288 (1989).
14. L. Scherk, "An Improved Value for the Electron Affinity of the Negative Hydrogen Ion," Can. J. Phys. 57, 558 (1979).

**Table 22 Parameters of the JHP 400-MeV proton linac (upgrade version).**

Plan-1 RFQ + DTL (50 MeV) + SDTL (149 MeV) + ACS (403 MeV)

Injection energy	3.0 MeV
Output energy	402.7 MeV
Frequency (RFQ, DTL, SDTL)	324 MHz
Frequency (ACS)	972 MHz
Total length (structure only)	149.3 m
Total length (including drift space)	205.0 m
Total rf driving power	41.7 MW
Beam power (30 mA)	12.0 MW
Beam power (60 mA)	24.0 MW
Total rf power (30 mA)	53.7 MW
Total rf power (60 mA)	65.7 MW

Plan-2 RFQ + DTL (50 MeV) + SDTL (202 MeV) + ACS (397 MeV)

Injection energy	3.0 MeV
Output energy	396.5 MeV
Frequency (RFQ, DTL, SDTL)	324 MHz
Frequency (ACS)	972 MHz
Total length (structure only)	154.7 m
Total length (including drift space)	217.1 m
Total rf driving power	42.0 MW
Beam power (30 mA)	11.8 MW
Beam power (60 mA)	23.6 MW
Total rf power (30 mA)	53.8 MW
Total rf power (60 mA)	65.6 MW

**Table 23 Parameters of the high-energy part from 149 to 403 MeV with ACS structure.**

Frequency	972	MHz
Injection energy	148.7	MeV
Output energy	402.7	MeV
Number of tank	48	
number of cells	872	
Structure length	82.8	m
Total length	117.1	m
Rf driving power (*)	27.7	MW
Beam power (30mA)	7.6	MW
Beam power (60mA)	15.2	MW
Total power (30mA)	35.3	MW
Total power (60mA)	42.9	MW
Accelerating field	4.1 - 4.7	MV/m
Energy gain	2.7 - 3.2	MeV/m
Drift space (**)	0.71 - 0.82	m

(\*) including a factor of 1.2.

(\*\*) shorter length is possible.

**Table 24 Parameters of the high-energy part from 203 to 397 MeV with ACS structure.**

Frequency	972	MHz
Injection energy	202.5	MeV
Output energy	396.5	MeV
Number of tank	36	
number of cells	624	
Structure length	61.8	m
Total length	92.9	m
Rf driving power (*)	20.7	MW
Beam power (30mA)	5.8	MW
Beam power (60mA)	11.6	MW
Total power (30mA)	26.5	MW
Total power (60mA)	32.3	MW
Accelerating field	4.3 - 4.7	MV/m
Energy gain	3.0 - 3.2	MeV/m
Drift space (**)	0.77 - 0.98	m

(\*) including a factor of 1.2.

(\*\*) shorter length is possible.

**Table 25 Parameters of the SDTL part from 50 to 149 MeV.**

Frequency	324	MHz
Injection energy	50.1	MeV
Output energy	148.7	MeV
Number of tank	21	
number of cells	105	
Structure length	39.5	m
Total length	56.0	m
Rf driving power (*)	10.1	MW
Beam power (30mA)	3.0	MW
Beam power (60mA)	5.9	MW
Total power (30mA)	13.0	MW
Total power (60mA)	16.0	MW
Number of klystron	6	
Accelerating field	3.86	MV/m
Energy gain	2.86 - 2.19	MeV/m
Drift space (**)	0.67-0.97	m

(\*) including a factor of 1.2.

(\*\*) shorter length is possible.

**Table 26 Parameters of the JHP 200-MeV proton linac.**

Injection energy	3.0	MeV
Output energy	202.5	MeV
Frequency	324	MHz
Particles	H <sup>-</sup>	
Peak current	30	mA
Beam width	400	μsec
Repetition rate	25	Hz
Average current	200	μA
Total length (structure only)	92.9	m
Total length (including drift space)	122.3	m
Total rf driving power	21.3	MW
Total rf power (30 mA)	27.3	MW
Total rf power (60 mA)	33.3	MW
Number of klystrons(*)	19	

(\*)includes for RFQ and debuncher

#### RFQ

Frequency	324	MHz
Injection energy	50	keV
Output energy	3	MeV

#### DTL

Frequency	324	MHz
Injection energy	3	MeV
Output energy	50.06	MeV
Number of tank	3	
number of cells	150	
Total length	28.51	m
Rf driving power (*)	3.92	MW
Beam power (30mA)	1.41	MW
Beam power (60mA)	2.82	MW
Total power (30mA)	5.33	MW
Total power (60mA)	6.74	MW
Number of klystron	3	
Acceptance		
A <sub>x</sub> (normalized 90%)	43	π mm-mrad
A <sub>y</sub> (normalized 90%)	41	π mm-mrad
A <sub>z</sub> (normalized 90%)	9.3	π MeV-deg
Focusing method	Equipartitioned focusing	
Stabilization	Post-stabilized	

DTL Tank number	1	2	3	
Injection energy	3.0	19.196	35.407	MeV
Output energy	19.196	35.407	50.058	MeV
Tank length	10.36	8.87	7.81	m
Number of cells	80	41	29	
Rf driving power (*)	1.16	1.36	1.40	MW
Beam power (30mA)	0.49	0.49	0.44	MW
Beam power (60mA)	0.98	0.98	0.88	MW
Total power (30mA)	1.64	1.84	1.84	MW
Total power (60mA)	2.08	2.33	2.28	MW
Accelerating field	2.5	2.7	2.9	MV/m
Stable phase	-30	-26	-26	
Drift space	4	3	0	$\beta\lambda$
	0.737	0.742		m

(\*) including a factor of 1.3

#### SDTL

Frequency	324	MHz
Injection energy	50.058	MeV
Output energy	202.488	MeV
Number of tank	31	
number of cells	155	
Structure length	65.9	m
Total length	92.4	m
Rf driving power (*)	17.4	MW
Beam power (30mA)	4.6	MW
Beam power (60mA)	9.2	MW
Total power (30mA)	22.0	MW
Total power (60mA)	26.6	MW
Number of klystron	14	
Accelerating field	3.86	MV/m
Energy gain	2.86 - 1.92	MeV/m
Drift space (**)	0.67-1.03	m
Acceptance		
$A_x$ (normalized 90%)	21.3	$\pi$ mm-mrad
$A_y$ (normalized 90%)	18.6	$\pi$ mm-mrad
$A_z$ (normalized 90%)	40.4	$\pi$ MeV-deg

(\*) including a factor of 1.2.

(\*\*) shorter length is possible.

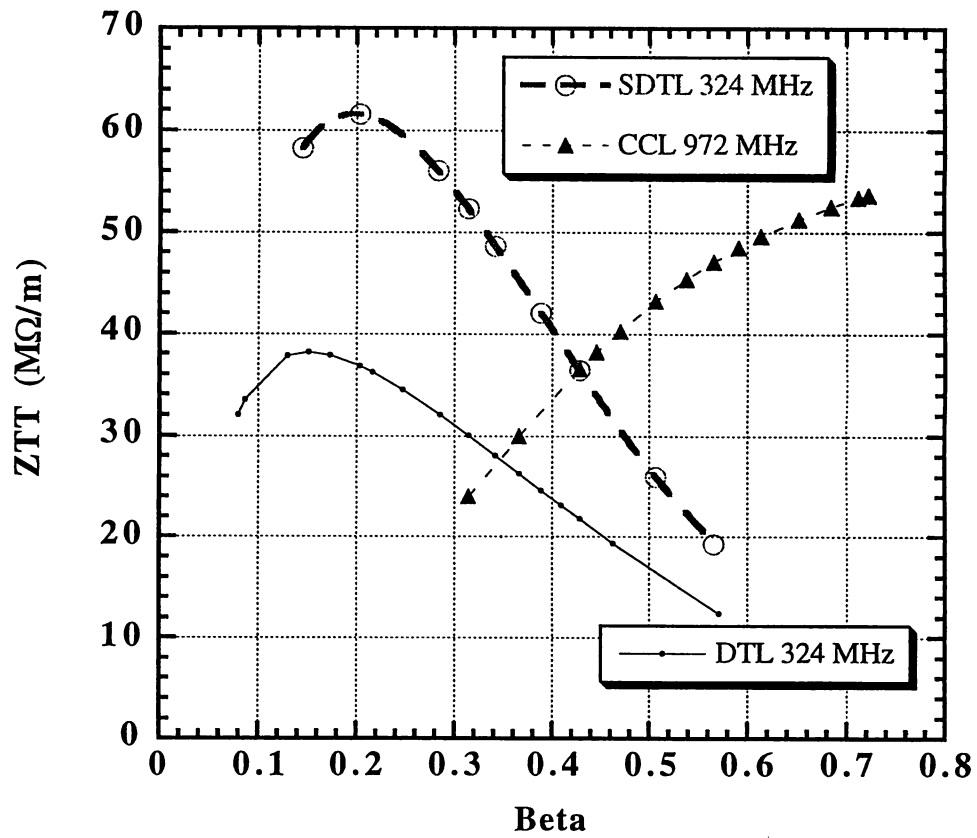


Fig. 50 Effective shunt impedances used for the JHP proton linac.